Mechanism of CO_2 and NH_3 Transport through Human Aquaporin 1: Evidence for Parallel CO_2 Pathways

Raif Musa-Aziz[1,2*], R. Ryan Geyer[2*], Fraser J. Moss[1‡], and Walter F. Boron[1,2,3‡]

[1]Department of Physiology and Biophysics, Institute of Biomedical Sciences, University of Sao Paulo.
[2]Department of Physiology and Biophysics, [3]Department of Medicine, and [4]Department of Biochemistry
Case Western Reserve University School of Medicine
Cleveland, OH 44106, USA.

Key words: *CO_2 permeability, osmotic water permeability, Surface pH, Xenopus laevis oocytes*

Running Title: *CO_2 pathways through AQP1*

For submission to: *The Journal of Physiology*

Author Contacts:

Raif Musa-Aziz

Department of Physiology and Biophysics
Institute of Biomedical Sciences
University of Sao Paulo
Sao Paulo, SP Brazil
Tel: 55-11-3091-7281
E-mail: raifaziz@icb.usp.br

R Ryan Geyer

E-mail: geyerro1976@gmail.com

‡ **Address correspondence to:**

Fraser J. Moss & Walter F. Boron

Department of Physiology and Biophysics
Case Western Reserve University School of Medicine
10900 Euclid Ave. Robbins Building E524
Cleveland, OH 44106-4970
Tel: 216-368-8978
E-mails: fraser.moss@case.edu & walter.boron@case.edu

Key Points

- Some membranes have little or no CO_2 permeability, absent protein channels like aquaporin-1 (AQP1).
- We confirm that, during CO_2 influx, AQP1 expression in *Xenopus* oocytes increases the magnitude of the resulting transient surface-pH increase by an amount $(\Delta pH_S^*)_{CO_2}$, measured with microelectrodes. During NH_3 influx, AQP1 expression increases the magnitude of the transient pH_S decrease by an amount $(\Delta pH_S^*)_{NH_3}$.
- p-chloromercuribenzene sulfonate (pCMBS), which reacts with C189 in the monomeric pore, reduces $(\Delta pH_S^*)_{CO_2}$ by half; $(\Delta pH_S^*)_{NH_3}$, to zero; and AQP1-dependent osmotic water permeability (P_f^*), by half.
- 4,4'-diisothiocyanatostilbene-2,2'-disulfonate (DIDS) reduces $(\Delta pH_S^*)_{CO_2}$ by half, but has no effect on $(\Delta pH_S^*)_{NH_3}$ or P_f^*. DIDS crosslinks AQP1 monomers expressed in *Pichia pastoris*.
- Together, pCMBS+DIDS reduces $(\Delta pH_S^*)_{CO_2}$ to zero. The C189S mutation of AQP1 eliminates the effects of pCMBS, but not DIDS. Our results thus show that CO_2 traverses AQP1 via the monomeric pore plus a novel, DIDS-sensitive route that may be the central pore.

Abstract

The traditional view had been that dissolved gases cross membranes simply by dissolving in and diffusing through membrane lipid. However, some membranes are impermeable to CO_2 and NH_3, whereas some aquaporin (AQP) water channels—tetramers with hydrophobic central pores—are permeable to CO_2, NH_3, or both. Nevertheless, we understand neither the routes that CO_2 and NH_3 take through AQP tetramers, nor the basis of CO_2/NH_3 selectivity. Here, we show—for human AQP1—that all NH_3 and about half the CO_2 pass through the hydrophilic, monomeric pores. Surprisingly, the remaining half of CO_2 takes another pathway. We expressed AQP1 in *Xenopus* oocytes and used microelectrodes to monitor surface-pH transients caused by CO_2 or NH_3 influxes. We found that p-chloromercuribenzene sulfonate (pCMBS)—which reacts with C189 in the monomeric pore—eliminates the entire NH_3 signal but only half of the CO_2 signal and osmotic water permeability of AQP1. 4,4'-diisothiocyanatostilbene-2,2'-disulfonate (DIDS), eliminates the remaining CO_2 signal but has no effect on NH_3 or osmotic water permeability. Together, the two drugs completely eliminate the CO_2 permeability of AQP1. When we express AQP1 in *Pichia pastoris*, treat spheroplasts with DIDS, and examine AQP1 by SDS-PAGE, reactivity with an anti-DIDS antibody shows that DIDS crosslinks AQP1 monomers. Our results provide the first evidence that a molecule can move through an AQP via a route other than the monomeric pore, and raise the possibility that selectivity depends on the extent to which CO_2/NH_3 move through monomeric pores vs. an alternate pathway (e.g., the central pore).

Introduction

Before the discovery of specific protein-mediated pathways in cell membranes, investigators had believed that small molecules (e.g., H_2O, urea, glycerol, lactic acid)—including CO_2—freely permeate all membranes to the extent that they can dissolve in and then diffusing through the lipid phase. Solubility-diffusion theory (S-DT) embodies this concept (reviewed in Boron, 2010; Michenkova *et al.*, 2021). For molecules other than dissolved gases, the generalizability of this notion faded with the discovery of each new membrane channel or transporter, consistent with the idea that cells evolved to achieve maximum-possible control over the transmembrane traffic of small molecules. We now believe that such traffic depends on some combination of membrane proteins (for which our understanding is understandably incomplete) and S-DT (responsible for non-specific leaks).

Regarding CO_2 traffic across biological membranes, the first inconsistency in the applicability of S-DT was the demonstration that apical membranes (i.e., facing the lumen) of single gastric glands are impermeable to CO_2 (Waisbren *et al.*, 1994). The second was the discovery that the human (h) aquaporin-1 (AQP1) not only conducts H_2O of course (Preston & Agre, 1991), but also CO_2 (Nakhoul *et al.*, 1998). Shortly after Nakhoul's observation, Cooper and Boron (1998) found that pCMBS inhibits CO_2 permeability in oocytes expressing wild-type (WT) AQP1. Prasad *et al.* (1998) then reported that AQP1 purified from human red blood cells (RBCs) and reconstituted into lipids from *E. coli* increases CO_2 permeability, an effect blocked by $HgCl_2$. Moreover, Forster *et al.* (1998) found that 4,4'-diisothiocyanatostilbene-2,2'-disulfonate (DIDS) applied to native human RBCs reduces not only HCO_3^- permeability, CO_2 permeability as well.

Forster and colleagues recognized that an explanation for their data could be that DIDS blocks a protein pathway for CO_2 diffusion through the RBC membrane. Indeed, Endeward *et al.* (2006) later found that AQP1 is responsible for about half of the CO_2 traffic across the RBC membrane, with the rhesus (Rh) complex's being responsible for most of the rest (Endeward *et al.*, 2008), leaving <10% to be accounted for by S-DT. Uehlein *et al.* (2003) reported that NtAQP1 in tobacco plants plays important physiological roles in CO_2 uptake—driven by a very small air-to-chloroplast gradient—for photosynthesis, stomatal opening, and leaf growth. Wang and colleagues demonstrated that the CO_2 permeability of tomato aquaporin PIP2;1 is essential for CO_2-dependent regulation of stomatal aperture (Wang *et al.*, 2016).

Besides H_2O and CO_2, various AQPs can conduct a variety of substances, including glycerol in the case of the aquaglyceroporin subfamily members (Gomes *et al.*, 2009). Regarding dissolved gases, hAQP1 conducts NH_3 (Nakhoul *et al.*, 2001) and NO (Herrera *et al.*, 2006). Moreover, different AQPs can exhibit strong selectivity for CO_2 over NH_3 or vice versa (Musa-Aziz *et al.*, 2009*a*; Geyer *et al.*, 2013). These results are consistent with the idea that cells, by regulating channel expression and trafficking to specific membranes, could control CO_2 or NH_3 permeability.

Structural studies show that AQP1 is a homotetramer with four independent monomeric pores—lined mainly by hydrophilic residues—that conduct H_2O (Walz *et al.*, 1997; Sui *et al.*, 2001). Between its monomers, AQP1 has a central pore—lined exclusively by hydrophobic residues—with no known function. Each monomer spans the lipid bilayer six times and has cytoplasmic amino and carboxyl termini. As predicted by the "hourglass model" (Preston & Agre, 1991), two consensus NPA motifs—on intracellular and extracellular loops that dip in towards the middle of AQP1, near the plane of the membrane—contribute importantly to the monomeric pore. The well-established reduction of osmotic water permeability (P_f) by $HgCl_2$ or pCMBS occurs as these agents react with cysteine-189 (C189), 2 residues upstream from the second NPA (Preston *et al.*, 1993). Replacing this cysteine with serine (C189S), which lacks a sulfhydryl group, eliminates this inhibition (Preston *et al.*, 1993).

We previously introduced an approach for using blunt, pH-sensitive microelectrodes to monitor transient changes in extracellular-surface pH (pH_S), caused by the entry of CO_2 or NH_3 into *Xenopus* oocytes heterologously expressing membrane proteins (Endeward *et al.*, 2006; Musa-Aziz *et al.*, 2009*b*, 2009*a*, 2010, 2014*a*). Mathematical modeling has elucidated the interpretation of CO_2-dependent pH_S transients (Somersalo *et al.*, 2012; Occhipinti *et al.*, 2014; Calvetti *et al.*, 2020). Using this pH_S approach in a survey of mammalian AQPs, we found that AQPs 1, 6, and 9 are permeable to both CO_2 (exposure to 5% CO_2) and NH_3 (0.5 mM NH_4Cl); AQP0, the M23 variant of AQP4 (AQP4-M23), and AQP5 are permeable to CO_2 but not NH_3; AQPs 3, 7, and 8 are permeable to NH_3 but not CO_2; and AQP2 as well as AQP4-M1 appear to be permeable to neither (Musa-Aziz *et al.*, 2009*a*; Geyer *et al.*, 2013). Using an osmotic-shrinkage assay with an 80-fold higher extracellular [NH_3] than in our studies, Assentoft et al detected NH_3 permeability through AQP4-M23 (Assentoft *et al.*, 2016). A key unanswered question is how various AQPs exhibit such strikingly different CO_2/NH_3 selectivities. The answer presumably lies in the pathways that these solutes take through various AQP tetramers. However, despite insights from

molecular-dynamics simulations (Wang *et al.*, 2007; Assentoft *et al.*, 2016), we still lack physiological evidence that establishes the pathways by which either CO_2 or NH_3 moves through any AQP. The purpose of the present study is to explore this problem.

Our approach was to use a combination of cell physiology and biochemistry. Heterologously expressing hAQP1 or its C189S mutant in *Xenopus* oocytes, and using the pH_S approach, we assessed the effects of pCMBS and DIDS on CO_2 and NH_3 permeation. We also assessed P_f so that we could normalize CO_2 and NH_3 data to H_2O permeability. We examine pCMBS because mercury—acting on monomeric pores—reduces both the P_f (Preston *et al.*, 1993) and CO_2 permeability of AQP1 (Cooper & Boron, 1998), as expressed heterologously in oocytes. We work with DIDS because this drug reduces CO_2 permeability in RBCs, and in oocytes expressing AQP1 (Endeward *et al.*, 2006). We find that virtually all of the hydrophilic NH_3 passes through the monomeric pore of hAQP1, whereas only about half of the more hydrophobic CO_2 travels via this pCMBS-sensitive pathway—the only established pathway through any AQP. The remaining half of the CO_2 moves through a different pathway that we can block with DIDS. Studies on hAQP1 expressed in *Pichia pastoris* indicates that DIDS crosslinks hAQP1 monomers. Our work is the first to demonstrate that a substance can move through an AQP via a pathway—possibly the hydrophobic central pore—that is distinct from the monomeric pore. Considering that mutations in human AQPs are associated with a wide variety of pathological conditions (see (Verkman, 2008; Verkman *et al.*, 2008), our work could lead to new insights into disease mechanisms, diagnostic tools, and therapeutic approaches for improving clinical outcomes.

Methods

For previous summaries of our approach in oocyte experiments, see Musa-Aziz et al. (2010, 2009a, 2009b). The following description is in far greater depth.

Ethical approval and animal procedures

The Institutional Animal Care and Use Committee at Case Western Reserve University approved the protocols for housing and handling of *Xenopus laevis* (approval # 2007-0134 and 2010-0147), used as a source of oocytes, and rabbits (approval # 2010-0146), for generating polyclonal antibodies.

Frogs. We purchased adult female *Xenopus laevis* frogs (NASCO Inc., Fort Atkinson, WI, USA) and housed them in a 20-gallon static aquarium, managed by the Animal Resources Center (ARC) of the School of Medicine. For stress mitigation, the tank had six or fewer frogs, and for environmental enrichment, we included a PVC elbow pipe. A charcoal Bio-Bag aquarium power pump (Tetra, Blacksburg, VA) circulated dechlorinated water through the tank. Three times per week, ARC staff fed the frogs with adult *Xenopus* diet (Zeigler Bros. Inc., Gardners, PA), sprinkling the food (10 pellets/frog) into the tank and, after a few hours when the *Xenopus* had fed, removing excess food with a net. As judged necessary, the ARC staff partially changed out water in the tank. Every 90 days, they moved the frogs into a newly cleaned tank that contained, in equal amounts, water from the previous tank and new de-chlorinated water.

We anesthetized frogs by immersion in a solution containing 0.2% tricaine (i.e., MS-222; ethyl 3-aminobenzoate methanesulfonate, catalog # A5040, Sigma-Aldrich, St Louis, MO, USA). When an animal became unresponsive to touch, we removed it from the solution and surgically extracted the ovaries. The animal was euthanized by cardiac excision prior to recovery from anesthesia.

In some experiments, we isolated oocytes from *Xenopus* ovarian lobes shipped overnight from NASCO.

Rabbits. We purchased adult female New Zealand white rabbits [1] from Charles River Laboratories (Ashland, OH). Following IACUC guidelines, ARC staff obtained a 5-mL pre-

[1] We code-named the rabbits, and the antisera they produced, “Ren” and “Stimpy.”

immune blood sample from an ear vein, and then inoculated two rabbits—gently restrained in a rabbit-restraint cage, and lightly sedated with intramuscular acepromazine (2 mg/kg)—with fresh DIDS-KLH fusion protein (see below) and Freund's complete adjuvant via subcutaneous injection on the back of the rabbit. A 10-mL sample of blood (via ear veins, alternating sides) was taken 14–21 days after the first boost, and the sera were evaluated for antigenicity towards proteins labeled with DIDS. Once a rabbit began producing sufficient titers of polyclonal anti-DIDS antibodies, staff collected 10 mL of blood per kg of body weight (~30–50 mL) at intervals of 21 to 30 days. After two of such larger blood collections, ARC staff euthanized the animals by cardiac excision and exsanguination, with blood from the terminal collection being transferred to our laboratory.

Solutions and chemicals

The compositions of our physiological solutions, made and used at room temperature (~22°C) were as follows:

ND96 solution. 96 mM NaCl, 2 mM KCl, 1.8 mM $CaCl_2$, 1 mM $MgCl_2$, 5 mM HEPES, adjusted to pH 7.50 with NaOH, osmolality 195 mOsm. We measured pH using a Ross electrode (catalog # 927007MD, Thermo Fisher Scientific, Waltham, MA, USA), a Dual Star pH meter (catalog # 8102BNUWP, Thermo Fisher Scientific), and calibrated with two standards (from Thermo Fisher Scientific), buffer solution pH 6.0 (catalog # SB104-1) and 8.0 (catalog # SB112-20). We measured osmolality with a vapor-pressure osmometer (catalog # 5520 Vapro, Wescor Inc., Logan, UT).

Ca^{2+}-free ND96 (for isolating oocytes). In this modified ND96 solution, we replaced 1.8 mM $CaCl_2$ with 2.7 mM NaCl.

OR3 media (for maintaining oocytes). For 2 liters of final solution, we added to 1.8 liters of H_2O one pack of powdered Leibovitz L-15 media with L-glutamine (catalog # L4386, Sigma-Aldrich), 100 mL of 10,0000 U/mL penicillin/streptomycin solution (cat # 15140122, Thermo Fisher Scientific) and 5 mM HEPES free acid. We then titrated the solution to pH 7.50 with NaOH, periodically measuring osmolality 195 mOsm, and sterile-filtered the solution using a Corning™ Disposable Vacuum Filter/Storage system (catalog # 09-761-107, Thermo Fisher Scientific), and stored it in a cold room for up to 2 weeks before use. Finally, just before use, we sterile-filtered a small volume of solution using a 60-mL syringe (catalog # 14-955-461, Thermo Fisher Scientific)

and a sterile in-line Nalgene filter with a 0.22-μm pore size and a 25-mm diameter (catalog # 723-9920, Thermo Fisher Scientific).

5% CO_2/33 mM HCO_3^- (for measuring ΔpHs due CO_2 influx). Here, 33 mM $NaHCO_3$ replaced 33 mM NaCl of the ND96 solution. After adding all components other than $NaHCO_3$, we titrated the solution to pH 7.50, then added the $NaHCO_3$, and then finally equilibrated the solution with 5% CO_2 (which brought pH back to 7.50).

0.5 mM NH_3/NH_4^+ in ND96 (for measuring ΔpH_S due NH_3 influx). We first made a variant of ND96 in which we replaced 5.0 mM NaCl with an equivalent amount of NH_4Cl, and then diluted this solution 1:10 into ND96.

Hypotonic ND96 (for measuring P_f): This was a variant of ND96 in which we reduced [NaCl] to lower osmolality to 80 mOsm/kg.

We used the following specialized chemicals:

pCMBS. In some experiments, we pre-incubated oocytes for 30 min in an ND96 containing 1 mM pCMBS (catalog # C367750, Toronto 196 Research Chemicals, North York, Ontario, Canada), a sulfhydryl reagent.

DIDS. In some experiments, we pre-incubated oocytes for 1 h in an ND96 containing 100 μM DIDS (catalog # D3514, Sigma-Aldrich], an amino-reactive agent.

BSA (Bovine serum albumin, to scavenge DIDS). In some experiments, after DIDS pretreatment, we washed off un-reacted DIDS by exposing oocytes to an ND96 to which we added 0.2% BSA (catalog # A9418, Sigma-Aldrich).

Oocyte Isolation

We performed the experiments presented in this paper at Case Western Reserve University between 2008 and 2013.

We placed ovarian lobes in a sterile 100-mm Petri dish containing ND96, cut them into irregular pieces (<1 cm on an edge) containing ~10 oocytes each using small iridectomy scissors, poured the mixture into a new Petri dish containing ~15 mL of Ca^{2+}-free ND96, gently agitated

the dish on a horizontal shaker[2] for 10 min, poured off as much liquid as possible, added fresh Ca^{2+}-free ND96, and repeated the pour/shake/wash cycle twice more. We then poured off the Ca^{2+}-free ND96, before adding ~15 mL of a freshly-made mixture of Ca^{2+}-free ND96 and 2 mg/mL Collagenase Type IA (catalog # C9722, Sigma-Aldrich), and gently agitating the dish on a horizontal shaker for 40 min. We next poured off the collagenase solution, added collagenase-free Ca^{2+}-free ND96, gently agitated the dish for 15 min, and repeated the pour/shake/wash cycle twice more. We then poured off the Ca^{2+}-free ND96, added ND96 (i.e., containing Ca^{2+}), gently agitated the dish on a horizontal shaker for 15 min, and repeated the pour/shake/wash cycle twice more. Finally, we poured off the ND96, added ~15 mL OR3 media, repeated the pour/wash cycle twice more, poured off most of the liquid, transferred the oocytes and remnant OR3 media to a fresh petri dish containing fresh OR3 media, and incubated the oocytes in an incubator at 18ºC. Later the same day, we used a stereomicroscope to sort the oocytes and select individual, defolliculated, mature oocytes (stage V/VI), which we immediately moved to a 6-well plate containing OR3 media (as many as ~50 oocytes/well), using a fire-sterilized transfer pipette prepared by using a diamond pencil to score the tapered end of a Pasteur pipette at a diameter large enough to accommodate an oocyte, breaking off and discarding the thin end of the pipette, fire-polishing the cut end of the pipette, and attaching the large end of the pipette to a manual, 2-mL Pipette Pump pipetter (catalog # S3-594-3, Thermo Fisher Scientific). We incubated the oocytes overnight at 18ºC before injection the following day with cRNA or H_2O (see below).

cRNA synthesis

The cDNAs encoding both hAQP1-WT (accession# NM_198098) and AQP1-C189S were gifts of Dr. Peter Agre (Johns Hopkins University). We subcloned the open reading frames of the constructs into the expression plasmid pGH19 (Trudeau *et al.*, 1995), a vector containing the 3′ and 5′ untranslated regions of the *Xenopus* laevis β-globin gene. In experiments in which we expressed AQP1-WT or AQP1-C189S in *P. pastoris*—as well as in some control experiments in

[2] In some later experiments, we instead put the oocytes and Ca^{2+}-free solution into 50-mL Falcon tubes (catalog # 14-959-49A, Thermo Fisher Scientific) and agitated them using a Tube Rotator (Scientific Equipment Products, Baltimore, MD).

oocytes—we added an N-terminal (Nt) FLAG-tag (MDYKDDDDKASEFKKKL… ; FLAG sequence, underscored; AQP1 sequence, double underscored).

We linearized cDNA constructs using NotI (for untagged AQP1-WT and AQP1-C189S) or XhoI (for the AQP1-FLAG tagged versions). The linearized DNA was then purified using the QIAquick PCR purification kit (catalog # 28104, Qiagen Inc., Valencia, CA). We then synthesized capped RNA (cRNA) using T3 (for untagged constructs; catalog# AM1348, Ambion, Austin, TX, USA) or T7 (for FLAG-tagged constructs; catalog# AM1344, Ambion) mMessage mMachine kits (Ambion, Austin, TX, USA). The cRNA was purified using the RNeasy MinElute RNA Cleanup Kit (catalog # 74204, Qiagen). The cRNA concentration was determined based on ultraviolet absorbance at 260 nm, and quality was assessed according the A260/280 ratio and gel electrophoresis.

Injection of oocytes with cRNA or water

One day after isolation and defolliculation, we injected stage V–VI oocytes with 25 nL of cRNA (1 ng/nl) encoding AQP1-WT, its C189S mutant, or the FLAG-tagged versions, or ~25 nL of water as a control. The injection apparatus consisted of a Nanoject II Variable Volume Automatic Injector (Drummond Scientific Company, Broomall, PA) connected to an injection needle that we pulled from 10-µl microdispenser capillary glass tubing (catalog # 3-000-210-G, Drummond), using a Model P-97 Flaming/Brown Micropipette Puller (Sutter Instrument Company, Novato, CA) and then modified by manually breaking the sealed end to yield a tip diameter of ~50-µm. After injection, we transferred oocytes to a 6-well plate (up to ~50/well) and incubated in OR3 media and maintained them for 3 days in an incubator at 18°C before use.

Electrophysiological recordings

For a schematic representation of the experimental chamber, position of the oocyte, and arrangement of electrodes, see figure 8b in Musa-Aziz *et al.* (2010).

Chamber and solution delivery. We placed oocytes into the channel (3 mm wide × 2 mm deep × 30 mm long) of a plastic perfusion chamber. We delivered the physiological solutions—or pH standards for calibrating pH microelectrodes at the outset of an experiment (see next section)—at a constant, total flow of 4 mL/min at room temperature (~22 °C), using a series of dual-syringe pumps (Model 22, Harvard Apparatus, South Natick, MA), each of which drove two 140-mL

plastic syringes (Sherwood Medical, St. Louis, MO) of identical content to deliver two solutions at 2 mL/min each.[3] The two solutions from each pump flowed through separate lengths of Tygon tubing (5/32-inch (~4.0 mm) outer diameter, 3/32-inch (~2.4 mm) inner diameter; Ryan Herco Products Corp., Burbank, CA; Formulation R3603-3; OD 4.8 mm /ID 1.6 mm) to two parallel assemblies of pneumatically operated 5-way valves (Clippard Instrument Laboratory, Cincinnati, OH), daisy-chained in such a way that we could switch among identical pairs of solution lines. The output of the parallel switching assemblies flowed into two lengths of Tygon tubing that carried the solutions to the vicinity of the chamber, where the two lines merged in a "mixing T", the output of which flowed into one end of the chamber channel. A suction device removed the solution at the opposite end of the channel. See Musa-Aziz *et al.* (2014) for details.

Measurement of membrane potential and intracellular pH. As described previously (Musa-Aziz *et al.*, 2010, 2014*a*), we impaled the oocyte (with the dark animal pole facing upward) with two microelectrodes, one for measuring membrane potential and the other for measuring intracellular pH. Both microelectrodes, with tip diameters of ~1 μm, we pulled from thin-walled borosilicate microfilament glass tubing (Catalog # G200TF-4, 2.0 mm OD ×1.56 mm ID, Warner Instruments Corporation, Hamden, CT), using the aforementioned P-97 microelectrode puller.

The microelectrodes for measuring membrane potential (V_m) we filled with 3 M KCl. We inserted an electrode into a half-cell/microelectrode holder (model # ESW-F20N, Warner Instruments Corp.), attached the holder to the V_m probe of an OC-725 two-electrode Oocyte Clamp (Warner Instruments Corp.), and mounted the probe on a model MM-33R micromanipulator (Warner Instruments Corp.). The V_m microelectrodes had resistances of ~0.3 – ~0.6 MΩ.

The microelectrodes for measuring intracellular pH (pH_i) were identical to the V_m electrodes except for the following fabrication process. In order to remove moisture, we placed the pulled micropipettes, with tips upwards, into the cylindrical holes of a reusable aluminum block (machined to create "legs" and thereby allow gases to circulate from beneath, and with smaller concentric cylindrical holes extending the entire height of the block to allow access of gases from

[3] We apparatus had this dual-solution arrangement to enable the use of out-of-equilibrium CO_2/HCO_3^- solutions in experiments that are not part of the present study.

below, to the interior of the glass capillary), placed the block into the bottom of a 100-mm Pyrex petri dish, covered the electrodes and block with an inverted 250-ml beaker, placed the petri dish on an open metal rack of an oven at 200 °C, and then baked overnight. With the microelectrodes still in the 200 °C oven, we then silanized them by tilting the beaker slightly and depositing 80 μL of *bis*-di-(methylamino)-dimethylsilane (Sigma-Aldrich, catalog #14755) between the legs of the aluminum block, releasing the breaker, and allowing the silane fumes to interact with the microelectrodes for 40 min before removing beaker. The silanized electrodes cured in the oven at 200 °C until ready for use. We used a hand-drawn, soft-glass pipette with a long tip to backfill each pH_i electrode with a liquid pH-sensitive sensor (catalog #95293, Hydrogen Ionophore I, mixture B, Fluka Chemical Corp., Ronkonkoma, NY), as described by (Ammann *et al.*, 1981), creating a column that extended ~1 mm from the microelectrode tip. We then backfilled an microelectrode with a buffer solution (containing, in mM, 40 KH_2PO_4, 23 NaOH, 15 NaCl, adjusted to pH 7.0), inserted the electrode into a half-cell/microelectrode holder (model # ESW-F20N, Warner Instruments Corporation), attached the holder to one probe of a model FD223 dual high-impedance electrometer, World Precision Instruments [WPI], Inc., Sarasota, FL), and mounted the probe on a model MM-33R micromanipulator (Warner Instruments Corp.). The pH_i microelectrodes had resistances of ~1.2 $10^{11}\Omega$.

After placing the tips of the V_m and pH_i microelectrodes in ND96 solution in the chamber channel (which we now refer to as the "bath"), we obtained V_m by electronically subtracting the system ground of the OC-725 amplifier from the signal of the V_m electrode. We obtained the voltage due to pH_i by electronically subtracting the signal of the V_m electrode from the signal of the pH_i electrode. For a schematic representation of the configuration of the electronics for obtaining V_m (this section) and the voltages due to pH_i (this section) and pH_S (next section), see figure 7c in Musa-Aziz *et al.* (2010). The device that performed the subtractions (Yale University Subtraction Amplifier, v3.1) also appropriately scaled the voltages for the inputs of an analog-to-digital converter, installed in a Windows-based computer. With the tips of the V_m and pH_i electrodes (and also the pH_S electrode, simultaneously; see next section) in the bath, we obtained the slope of the pH_i electrodes as we used the aforementioned solution-delivery system (see previous section) to flow a pH standard at pH 6.0 (catalog # SB104-1) continuously through the chamber channel, recorded the voltage due to that pH, used the valve system to switch the flowing solution to a second, pH-8.0 standard (catalog # SB112-20), and then recorded the corresponding

voltage. We typically switched between standards in a pH-6→8→6→8 sequence, accepting pH_i microelectrodes that completed their electrical response—which also included the time for the solution in the chamber channel to fully change composition—within ~5 s (~2 s for pH_S electrodes) and had slopes in the range of 53 to 60 mV/pH unit. After the recordings in the final pH-calibration solution, we re-introduced the ND96 solution into the bath, and then added the oocyte to the chamber channel. After impaling the oocyte with the V_m electrode, and with the tip of the pH_i electrode near the oocyte, we obtained a single-point pH calibration of the pH_i microelectrode in the ND96 solution (defined as having a pH 7.50). We then impaled the oocyte with the pH_i microelectrode. After stabilization, oocytes had spontaneous V_m values at least as negative as –40 mV. We continuously recorded pH_i to judge the integrity of the oocyte and compare the pH_i time course with that of surface pH. In the present paper, we are not presenting the pH_i data, which nevertheless are similar to those of our previous studies (Musa-Aziz *et al.*, 2009*a*, 2010, 2014*a*, 2014*b*).

Measurement of surface pH. We measured surface pH with liquid-sensor pH microelectrodes that we fabricated and employed in the same way as we did for pH_i microelectrodes (see above), but with four differences. First, we pulled the pH_S microelectrodes from standard-walled (rather than thin-walled) borosilicate microfilament glass tubing (Part No. G200F-4, 2.0 mm OD ×1.16 mm ID, Warner Instruments). Second, we used a microforge to break off and fire polish the tips (inner diameter ≅ 20 μm at tip) as one would for a giant-patch pipette (Musa-Aziz *et al.*, 2010). It was to facilitate the fire polishing that we used the standard-walled glass tubing. Third, we used a vented microelectrode holder (model # ESW-F20N, Warner Instruments Corp.) mounted on a model MM-33L micromanipulator. The vent prevented pressure buildup that would otherwise have pushed the liquid pH sensor out of the wide electrode tip as we pushed the pH_S electrode into the holder. Note that we attached the microelectrode holder of the pH_S electrode to the second of two inputs of the FD223 electrometer. And fourth, after obtaining the pH_S-electrode slope (which we did at the same time as obtaining the pH_i electrode slope, as described above) and single-point calibration of the pH_S electrode in ND96, we used an ultra-fine computer-controlled micromanipulator (model MPC-200 system, Sutter Instrument Company) to positioned the blunt tip of the pH_S electrode near the oocyte's equator (i.e., between the upward-facing animal pole and downward-facing vegetal pole), and ~5 degrees behind the meridian (i.e., barely in the "shadow" of the flowing extracellular solution) until the pH_S electrode tip just touched

the surface of the oocyte (Musa-Aziz *et al.*, 2010, 2014*a*). We then further advanced the tip by ~40 μm to create a slight dimple in the membrane. Periodically during the experiment (indicated by vertical gray bands in each panel of Figure 2*B*, Figure 3, and Figure 6), we withdrew the electrode 200 – 300 μm from the oocyte for recalibration in the bulk extracellular fluid (bECF) of the bath (i.e., pH 7.50).

The external reference electrode for the pH_S measurement was a calomel half-cell, bridged to the chamber channel via a long glass micropipette filled with 3M KCl, connected to a model 750 electrometer (WPI), and positioned so that its tip was just downstream of the oocyte. We obtained pH_S signal by electronically subtracting the calomel signal from the signal of the pH_S electrode.

We established a virtual ground with an Ag/AgCl half cell (connected to the ISense input of the voltage-clamp amplifier) bridged to the chamber by a second glass microelectrode filled with 3M KCl, and positioned the tip of this second bridging pipette close to that of the first, that is, just downstream of the oocyte.

Measurement of osmotic water permeability. We measured P_f as described by (Zhang *et al.*, 1990; Preston *et al.*, 1992, 1993). Using an approach similar to those in previous studies by our group (Virkki *et al.*, 2001; Musa-Aziz *et al.*, 2009*a*), we dropped an oocyte into a Petri dish containing a hypotonic solution (80 mOsm) to induce cell swelling and, while illuminating from beneath the dish, used a video camera to obtain images of the oocyte (1/s × 60 s). Using a small metal sphere next to the oocyte as a size reference, we determined the projection areas of the oocyte, and—assuming the oocyte to be a perfect sphere—computed idealized oocyte volume (V_{Oocyte}) and idealized oocyte surface area as a function of time. We estimated the actual surface area (S, in cm^2) by multiplying the idealized surface area by a factor of 9. We computed P_f from the following equation:

$$P_f = \underbrace{\frac{\left(\frac{dV_{Oocyte}}{dt}\right)_{max}}{S \times \Delta Osm \times V_W}}_{\text{units: } cm\,/\,s},$$

the form of which differs slightly from that of Zhang *et al.*, (1990).[4] Here, $(dV_{Oocyte}/dt)_{max}$ is the maximum time rate of change of cell volume (i.e., the maximal H_2O influx, or $J_{V,max}$, in $cm^3\ s^{-1}$), ΔOsm is the initial osmotic gradient across the oocyte membrane (i.e., 195 – 80 = 115 mOsm, expressed as mol cm^{-3}), and V_w is the molar volume of water (18.1 $cm^3\ mol^{-1}$). As for the electrophysiological studies, we performed all P_f assays at room temperature (~22 °C).

Protocols for physiological experiments

Figure 1*A–H* illustrates the sequence of events in our experimental protocols.

Electrophysiological assays. On the day of an experiment, we followed an 10-step protocol:

(A) Use a transfer pipette to pick up an untreated oocyte from a well of a 6-well plate (each well containing OR3 medium + ~30 oocytes, all injected with the same material) and drop the oocyte into a petri dish containing ND96. After flushing the transfer pipette tip several times with ND96 (to remove OR3), we …

(B) Use the transfer pipette to move the washed oocyte to an identified well of a 24-well plate (1 oocyte/well) containing ND96. Repeat this procedure for several oocytes, each of which will remain in its well (1–3 hours) until we …

(C) Use the transfer pipette to place the oocyte in the chamber, begin flowing ND96, and measure V_m, pH_i, and pH_S under basal conditions.

(D) Monitor pH_S as we replace ND96 with either the CO_2/HCO_3^- solution (as in Figure 2*B*, Figure 3) or the NH_3/NH_4^+ solution (as in Figure 5*B*, Figure 6); all oocytes in the study underwent this control assay.

---

[4] To obtain P_f in the proper units ($cm\ s^{-1}$) in the above equation, the derivation by Zhang *et al.*, (1990) requires that the division of "moles of osmotically active particles" (in the ΔOsm term) by "moles of water" (in the V_W term) yield a numerical result that is unitless, which of course is impossible. This inconsistency arises during the derivation of the water-flux equation when one switches from describing the energy of water (i.e., RT) as "per mole of water" per se to the energy of water "per mole of osmotically active solute" during the introduction of the Van't Hoff equation. The introduction of a phantom conversion factor with a value of unity—but with the units "(per mole of osmotically active solute)/(per mole of water)"—eliminates the inconsistency.

(E) Immediately upon completion of the pH_S assay, use a transfer pipette to return the oocyte from the chamber to its original well and incubate the oocyte at ~22°C in ND96. We serially process all oocytes from a 24-well plate up to this stage (i.e., steps 'C' through 'E') and then pause. Thus, this second period of incubation in ND96 (step 'E') ranges from ~30 min to ~3 h.

(F) Use a transfer pipette to move each oocyte in the 24-well ND96 plate to a corresponding well in one of three new 24-well plates. Here, the wells contain one of the following three solutions: (F_1) 1 mM pCMBS dissolved in ND96 (30 min incubation; see Figure 3*DEF*, Figure 6*DEF*, Figure 7, Figure 8, or Figure 9*CD*); (F_2) 100 μM DIDS dissolved in ND96 (60 min incubation; see Figure 3*GHI* or Figure 6*GHI*); or (F_3) ND96 without an added drug ("sham").

(G) Wash the oocyte. Except in a few cases (see indented paragraph below), we wash the oocyte ×3 in a petri dish containing ordinary ND96, as follows. We use a transfer pipette to pick up an oocyte from a 24-plate (step 'F') and release the oocyte into a petri dish containing ND96, quickly pick up and released the oocyte into this wash solution twice more (to remove excess drug, if present). At this point, most oocytes progress immediately through step 'H' (below). However, in a minority of experiments (see Figure 3*JKL*), we serially treated oocytes with both pCMBS and DIDS. Here, oocytes previously treated with pCMBS (step 'F_1') we exposed to DIDS, as indicated by steps $\alpha_1 \rightarrow \alpha_2 \rightarrow \alpha_3$. Conversely, oocytes previously treated with DIDS (step 'F_2') we exposed to pCMBS, as indicated by steps $\beta_1 \rightarrow \beta_2 \rightarrow \beta_3$. In one experiment without any drugs, we also followed the steps $\gamma_1 \rightarrow \gamma_2 \rightarrow \gamma_3$ ("double sham").

> Not illustrated in Figure 1 is a protocol variant that we employ in a few cases (i.e., Figure 9*AB/right bars*) in which we introduce an additional step between 'F_2' and 'G'. Here, after treating an oocyte with DIDS (step 'F_2'), we scavenge unreacted DIDS with albumin as follows. After using a transfer pipette to pick up the oocyte from the DIDS-containing ND96 solution, we release the oocyte into a petri dish containing <u>0.2% albumin</u> in otherwise DIDS-free ND96, and allow the oocyte to remain in the albumin solution ×20 min. We then wash off the albumin in step 'G' by transferring the oocyte to a petri dish containing ordinary ND96, and pick up and release the oocyte ×3 using a transfer pipette.

(H) Use a transfer pipette to move the oocyte from the petri dish (step 'G') to an identified well in one of three new 24-well plates, all containing ND96, in preparation for the next assay.

(I) Transfer the oocyte back to the chamber and (as in step 'C'), and again measure the new basal V_m, pH_i, and pH_S.

(J) Monitor (as in step 'D'), for the second time, the pH_S transient as we replace ND96 with the CO_2/HCO_3^- (or NH_3/NH_4^+) solution.

Thus, oocytes in the top row of Figure 3 (i.e., Figure 3*ADGJ*) went through one of the following three sequences: Panels *A*→*D*, *A*→*G*, or *A*→*J*, which requires 12–22 h for an entire group of 24 oocytes in a day's work. Not all oocytes survived the entire protocol (as judged by the color/integrity of the animal pole).

***P_f* assays.** We performed P_f assays on separate oocytes from the same oocyte batch (i.e., oocytes prepared from the same ovary) used in our pH_S assays. On the same day as pH_S experiments, we: (1) Use a transfer pipette to remove 6 untreated oocytes of each experimental group—hAQP1, C189S mutant, or hAQP1 FLAG-tagged—from an identified 6-well plate containing ND96 solution (i.e., a total of 18). (2) Place the oocytes—as quickly as possible—in a Petri dish containing hypotonic ND96. (3) Use a video camera (described above) to monitor cell swelling; oocytes of each group underwent this control assay. (4) Immediately remove the oocytes from the hypotonic solution to identified wells in another Petri dish containing standard ND96 solution to wash the oocytes ×3 at ~22°C (described above under electrophysiological assays). (5) Incubate at ~22°C either for (5a) 30 min in ND96 containing 1 mM pCMBS, or (5b) 1 hour in ND96 containing 100 μM DIDS. (6) Wash the oocytes (as described under electrophysiological assays, point '5a'). (7) Transfer the oocytes to a Petri dish containing hypotonic, drug-free ND96 as in '2' above. (8) Monitor swelling as in '3' above.

Generation of the DIDS antibody

Generation of DIDS-fusion protein. We used rabbits to produce polyclonal antibodies against DIDS, as described by Garcia & Lodish (1989). Briefly, we reacted 2.4 mM DIDS (catalog # D3514, Sigma-Aldrich), with 5 mg keyhole limpet hemocyanin (KLH;, catalog # H7017, Sigma-Aldrich) in 500 μL of phosphate buffer saline (PBS; i.e., 150 mM NaCl, 10 mM phosphate buffer, pH 7.0) in the dark at 37°C × 40 min. Afterwards, we centrifuged the sample × 30 s in an Eppendorf benchtop centrifuge (catalog # 5415C, Thermo Fisher Scientific) to remove large insoluble aggregates After pooling yellow supernatants from several centrifuge tubes, we dialyzed against

PBS at 4°C overnight in a slide-a-lyzer dialysis cassette (Thermo Fisher Scientific). The following day, we removed the KLH-DIDS sample from the cassette; quantified the DIDS by absorbance spectroscopy at 340 nm, assuming a molar extinction coefficient (ε) of 54,000 M^{-1} cm^{-1}; aliquoted the dialyzed KLH-DIDS solution; and immediately used it for immunization.

For each rabbit, we separately processed each of three blood samples (see above)—2 lots of ~30–50 mL plus the terminal sample. We centrifuged the blood for 10 min at 1000 ×g using an Eppendorf bench top centrifuge to isolate the serum, and then evaluated antigenicity on western blots of DIDS-labeled AQP1. We purified the antibodies (mainly IgG) from the remainder of the serum using a Protein A column (Catalog # 20356, ThermoFisher Scientific), following the manufacturer's instructions; estimated [IgG] by measuring absorbance at 280 nm (assuming ε = 210,000 $M^{-1}cm^{-1}$) using a NanoDrop 2000c spectrophotometer (ThermoFisher Scientific); separated the material into aliquots corresponding to 1 mg/mL of anti-DIDS antibody; and stored the aliquots at either –20°C for short-term storage or –80°C for long-term storage.

Biochemical experiments

Isolation of oocyte membranes. We used a previously described method (Leduc-Nadeau *et al.*, 2007), except that, after disrupting oocytes and centrifuging, we removed the supernatant and added fresh buffer to the pellet, repeating the procedure until the supernatant was clear (i.e., void of yolk).

Purification of oocyte membrane proteins. We resuspended isolated oocyte membranes in Tris-Buffered Saline (TBS, 50 mM Tris HCl, pH 7.4, 150 mM NaCl) + 2% n-dodecyl-β-D-maltopyranoside (DDM; Sol-Grade, catalogue #D310S, Anatrace, Maumee, OH), incubated at 4°C × 2h, centrifuged at 16,000 × g at 4°C × 30 min, and then collected the supernatant containing the solubilized membrane proteins and diluted it so that [DDM] was ≤ 0.5%.

Overexpression of AQP1-FLAG in *Pichia pastoris*. We ligated N-terminally FLAG-tagged hAQP1 (MDYKDDDDKASEFKKKL… ; FLAG sequence underscored, hAQP1 sequence double underscored) into the pPICZ-A vector (Invitrogen, Carlsbad, CA), induced protein expression with methanol × 72 hours at 26ºC, harvested the yeast by centrifugation, and obtained and spheroplasts using zymolyase treatment. We then equally divided the spheroplasted cells into two groups (i.e., no DIDS and added 100 μM DIDS), incubated × 1 hour at ~22°C, and then solubilized overnight

at 4°C in TBS + 2% DM, with cOmplete™ Protease Inhibitor Cocktail (catalog #11697498001, Roche, Mannheim, Germany). Following membrane solubilization, we clarified the material by low speed centrifugation, mixed with anti-FLAG resin (catalog #A2220, Sigma-Aldrich), and eluted proteins from a column using TBS + 0.1% DM + 500 µg/mL FLAG peptide (catalog #F4799, Sigma-Aldrich) at pH 7.4. In some cases, we subjected FLAG-purified AQP1 to size-exclusion chromatography using a Sephadex 75 column.

Western blotting of membrane proteins from oocytes or *Pichia pastoris*. We separated proteins extracted from oocyte membranes by SDS-PAG using Tris-Glycine 4–20% gels (BioRad Laboratories, Hercules, CA) or proteins from extracted from *Pichia* membranes using 12% Tris-Glycine gels; transferred the proteins to polyvinylidene difluoride (PVDF) membranes using an iBlot 7-Minute Blotting System (Thermo Fisher Scientific); and subsequently blocked the cross-linked proteins with Tris-buffered saline with tween (TBST), comprising 25 mM Tris at pH 7.4, 150 mM NaCl, 0.05% Tween-20 (catalog # P9416, Sigma-Aldrich) + 5% milk powder × 1h.

We probed blots from oocytes samples with a polyclonal anti-AQP1 (catalog # AQP11-A, Alpha Diagnostics, San Antonio, USA), and blots from *P. pastoris* samples with monoclonal anti-FLAG (catalog # F3165-2MG, Sigma-Aldrich) or polyclonal anti-DIDS (made in-house, see above), applying all primary antibodies at 1:1000 in TBST + 5% milk, at 4°C overnight. The next day, we washed the blot ×5 with TBST × 10 min. We detected the primary polyclonal antibodies (i.e., anti-AQP1 and anti-DIDS) with an HRP-conjugated goat anti-rabbit secondary antibody (catalog # 1706515, BioRad Laboratories), and detected the primary monoclonal antibody (i.e., anti-FLAG), an HRP-conjugated goat anti-mouse secondary antibody (catalog # STAR207P, BioRad Laboratories). We applied both secondary antibodies at 1:5000 in TBST × 1h, washed the blot ×5 with TBST × 10 min, developed the immunoblots using ECL Prime Western Blotting Detection Reagent (catalog # 12316992, GE Healthcare Amersham, Piscataway, NJ), acquired images with a Typhoon Trio gel-documentation system (GE Healthcarefryan), and evaluate band density patterns using Image J software (NIH, Bethesda, MD).

Statistics

We present data as the mean ± SD (standard deviation), and define the n as number of replicate experiments (i.e., oocytes). Statistical comparisons were made using a one-way ANOVAs among all groups, followed by Student-Newman-Keuls analyses.

Results

Surface-pH Measurements for AQP1-WT and AQP1-C189S

pH_S measurements for CO_2 transport. Figure 2*A* is a schematic representation of the reaction and diffusion events that take place as we switch the bath solution—that is, the bulk extracellular fluid—from ND96 to another that contains 5% CO_2/33 mM HCO_3^- at a constant pH of 7.50. This solution change not only leads to a net influx of CO_2 that lowers intracellular pH (Roos & Boron, 1981) but also lowers CO_2 concentration near the outer surface of the cell membrane ($[CO_2]_S$). This decrease in $[CO_2]_S$ has two effects. First, it creates a gradient for CO_2 diffusion from the bECF to the cell surface, which by itself has no effect on pH. Second, it drives the reactions $HCO_3^- + H^+ \rightarrow H_2CO_3 \rightarrow CO_2 + H_2O$ at the cell surface, thereby replenishing CO_2 and causing an alkaline pH_S transient, the maximal excursion of which we define as ΔpH_S (Endeward *et al.*, 2006; Musa-Aziz *et al.*, 2009*a*; Geyer *et al.*, 2013). Our colleagues have used 3D reaction-diffusion models to simulate these pH_S and pH_i changes as CO_2 diffuses into a spherical cell (Somersalo *et al.*, 2012; Musa-Aziz *et al.*, 2014*a*, 2014*b*; Occhipinti *et al.*, 2014; Calvetti *et al.*, 2020).

Figure 2*B* shows a representative pH_S recording from a H_2O-injected or "control" oocyte during such a solution change. (for solution composition, see Methods). The vertical gray bands in the figure indicate periods during which we withdraw the tip of the extracellular pH microelectrode from its previous position, in which its tip created a small dimple (~40 μm) in the oocyte surface, to a distance of 200 – 300 μm for recalibration in the bECF, which we assume to have a pH of precisely 7.50. We describe the recalibration in the legend of Figure 2.

Figure 2*C* shows a representative western blot of membrane preparations (see Methods) of oocytes injected with H_2O or cRNA encoding either AQP1-WT or AQP1-C189S. The lower band(s) at ~25 kDa presumably represents unglycosylated or core-glycosylated AQP1 in the endoplasmic reticulum. The upper bands at ~37 kDa represent mature-glycosylated AQP1, much of which is presumably at the plasma membrane. Assuming that the AQP1 antibody has similar sensitivities for the WT and C189S proteins, we conclude that *Xenopus laevis* oocytes express similar amounts of each.

Figure 3 shows a series of 12 representative pH_S recordings, the first of which, in Figure 3*A*, is a replicate of Figure 2*B*. We can see that the ΔpH_S induced by the CO_2 influx in this H_2O-injected control oocyte is much smaller (Figure 3*A*) than in a day-matched oocyte injected with cRNA encoding hAQP1-WT (Figure 3*B*).

We define $(\Delta pH_S^*)_{CO_2}$ as the difference between the CO_2-induced ΔpH_S value of an oocyte expressing a channel protein (e.g., Figure 3*B*) and the mean ΔpH_S for all day-matched control oocytes (e.g., Figure 3*A*). This difference is a semiquantitative index of the channel-specific CO_2 flux (Musa-Aziz *et al.*, 2009*a*; Somersalo *et al.*, 2012; Calvetti *et al.*, 2020). The leftmost bar in Figure 4*A* represents the mean $(\Delta pH_S^*)_{CO_2}$ value for 30 oocytes expressing AQP1-WT in the absence of inhibitors.

To assess the importance of the monomeric pore, we examined the effect of pCMBS, which, like $HgCl_2$, covalently modifies Cys-189 near the extracellular entrance of the monomeric pore and reduces the component of P_f due to AQP1 (Preston *et al.*, 1993), which we define as P_f*. Preston et al showed that $HgCl_2$ has no effect on P_f if oocytes express the C189S mutant of AQP1 (Preston *et al.*, 1993). On the basis of pH_i measurements, (Cooper & Boron (1998) showed that pCMBS significantly reduces the CO_2 permeability of oocytes expressing AQP1-WT, but that this effect is absent oocytes expressing AQP1-C189S. In the present study, in which we now monitor pH_S, experiments on individual oocytes confirm that pretreatment with 1 mM pCMBS (see Methods) reduces the CO_2-induced ΔpH_S in an AQP1-WT oocyte (Figure 3*E* vs. *B*) but not in an oocyte expressing AQP1-C189S (Figure 3*F* vs. *C*). pCMBS has no effect on a H_2O-injected oocyte (Figure 3*D* vs. *A*), for which ΔpH_S is already small. We conclude that pCMBS reduces but does not eliminate the ΔpH_S due to AQP1 (Figure 3*E* vs. *D*).

The leftmost bar in Figure 4*B* represents the mean $(\Delta pH_S^*)_{CO_2}$ from 22 oocytes expressing AQP1-C189S in the absence of inhibitors. This $(\Delta pH_S^*)_{CO_2}$ value is very similar to that for oocytes expressing AQP1-WT (leftmost bar in Figure 4*A*). A comparison of the first and second bars in Figure 4*A* and *B* shows that pCMBS reduces $(\Delta pH_S^*)_{CO_2}$ by about half in oocytes expressing AQP1-WT, but has no significant effect in AQP1-C189S oocytes. These data support the hypothesis that, of the CO_2 that transits AQP1, a major component moves through the same monomeric pores as H_2O.

While studying HCO_3^- transport, Forster et al unexpectedly found that DIDS blocks a large fraction of CO_2 permeability of human RBCs (Forster *et al.*, 1998). Endeward et al found that, in RBCs genetically deficient in AQP1, DIDS has a reduced effect on CO_2 permeability (Endeward *et al.*, 2006). Here, in experiments on single oocytes, we find that pretreatment with 100 μM DIDS reduces the CO_2-induced ΔpH_S in both an AQP1-WT oocyte (Figure 3*H* vs. *B*) and an AQP1-C189S oocyte (Figure 3*I* vs. *C*), but not in a H_2O-injected oocyte (Figure 3*G* vs. *A*), for which ΔpH_S is already small.

The third bars in Figure 4*A* and *B* summarize mean $(\Delta pH_S^*)_{CO_2}$ values from a larger group of oocytes pretreated with DIDS. A comparison of the first and third bars shows that DIDS reduces $(\Delta pH_S^*)_{CO_2}$ by at least half in oocytes expressing either AQP1-WT (Figure 4*A*) or AQP1-C189S (Figure 4*B*). These data are consistent with the hypothesis that a significant fraction of CO_2 moves through AQP1 by a DIDS-sensitive pathway that is unaffected by the C189S mutation in the extracellular mouth of the monomeric pore.

Returning to experiments on individual oocytes, we see that the sequential exposure of an AQP1-WT oocyte to pCMBS and then DIDS substantially reduces the CO_2-induced ΔpH_S (Figure 3*K* vs. *B*). Moreover, and the size of the ΔpH_S for the pCMBS/DIDS-treated AQP1-WT oocyte (Figure 3*K*) is about the same as for H_2O-injected oocytes ±inhibitors (Figure 3*A,D,G,J*). In an AQP1-C189S oocyte, the combination of pretreating with pCMBS then DIDS reduces the CO_2-induced ΔpH_S (Figure 3*L* vs. *C*), but by no more than DIDS alone (Figure 3*I* vs. *C*).

The fourth bars in Figure 4*A* and *B* summarize mean $(\Delta pH_S^*)_{CO_2}$ values from a larger group of oocytes, in experiments in which we treated with pCMBS and DIDS in either order. A comparison of the first and fourth bars shows that pCMBS+DIDS reduces $(\Delta pH_S^*)_{CO_2}$ by slightly more than 100% in AQP1-WT oocytes (Figure 4*A*). In the AQP1-C189S oocytes, pCMBS+DIDS reduces $(\Delta pH_S^*)_{CO_2}$ to about the same extent as DIDS alone (Figure 4*B*), about 40%. Taken together, the data in Figure 3 and Figure 4*A* and *B* are consistent with the hypothesis that, in addition to the component of CO_2 that moves through the four monomeric pores, another component—at least as large—moves through an entirely separate, DIDS-sensitive pathway.

pH_S measurements for NH_3 transport. Figure 5*A* is a schematic representation of the reaction and diffusion events that take place as we exposed an oocyte to a solution containing 0.5 mM NH_3/NH_4^+. Here, the changes in pH_S are opposite in direction to those caused by CO_2/HCO_3^-

exposure. As the weak base NH_3 enters the cell, it causes a decrease in $[NH_3]_S$, which has two effects. First, it provides a gradient for NH_3 diffusion from the bECF to the cell surface. By itself, this diffusion has no effect on pH. Second, the decrease in $[NH_3]_S$ also drives the reaction $NH_4^+ \rightarrow NH_3 + H^+$ at the cell surface, replenishing NH_3 and producing an acidic pH_S transient (Musa-Aziz *et al.*, 2009*b*, 2009*a*), so that $\Delta pH_S < 0$. Figure 5*B* shows a representative pH_S recording as we introduce NH_3/NH_4^+.

Figure 6 shows a series of 9 representative pH_S recordings on individual oocytes, the first of which, in Figure 6*A*, is a replicate of Figure 5*B*. We find that the NH_3-induced '$-\Delta pH_S$' is much smaller in the H_2O-injected oocyte (Figure 6*A*) than in a day-matched oocyte expressing AQP1-WT (Figure 6*B*). Subtracting the ΔpH_S from the H_2O-injected oocyte from the ΔpH_S from the AQP1-WT oocyte yields the channel-dependent, NH_3-induced ΔpH_S—$(\Delta pH_S^*)_{NH_3}$ (Musa-Aziz *et al.*, 2009*a*). The leftmost bar in Figure 7*A* represents the mean $(\Delta pH_S^*)_{NH_3}$ for 18 oocytes expressing AQP1-WT in the absence of inhibitors.

In experiments on representative oocytes, we find that pretreating an AQP1-WT oocyte with 1 mM pCMBS markedly reduces '$-\Delta pH_S$' (Figure 6*E* vs. *B*), but has no effect in an AQP1-C189S oocyte, where '$-\Delta pH_S$' remains high (Figure 6*F* vs. *C*); or in a H_2O oocyte, where '$-\Delta pH_S$' remains low (Figure 6*D* vs. *A*). The leftmost bar in Figure 7*B* represents the mean $(\Delta pH_S^*)_{NH_3}$ value from 11 oocytes expressing AQP1-C189S in the absence of inhibitors. This $(\Delta pH_S^*)_{NH_3}$ value is virtually identical to that for oocytes expressing AQP1-WT (leftmost bar in Figure 7*A*). A comparison of first and second bars shows that pCMBS reduces '$-(\Delta pH_S^*)_{NH_3}$' by virtually 100% in oocytes expressing AQP1-WT (Figure 7*A*), but has no effect in AQP1-C189S oocytes (Figure 7*B*).

Returning to experiments on individual oocytes, we see that DIDS has no effect on '$-\Delta pH_S$' in a H_2O-injected control oocyte (Figure 6*G* vs. *A*), where '$-\Delta pH_S$' remains low; or in an AQP1-WT oocyte (Figure 6*H* vs. *B*) or an AQP1-C189S oocyte (Figure 6*I* vs. *C*), where '$-\Delta pH_S$' remains high. The third bars in Figure 7*A* and *B* summarize mean $(\Delta pH_S^*)_{NH_3}$ values from larger groups of DIDS-pretreated oocytes. A comparison of the first and third bars in each panel shows that DIDS is without effect on $(\Delta pH_S^*)_{NH_3}$ in oocytes expressing AQP1-WT (Figure 7*A*) or AQP1-C189S (Figure 7*B*). Taken together, the data in Figure 6 and Figure 7 indicate that all of the NH_3 transiting AQP1 moves via the same pathway as H_2O and a major component of CO_2—namely the four

pCMBS-sensitive monomeric pores. None of the NH_3 moves via the alternate, DIDS-sensitive pathway taken by the other major component of CO_2.

Cell-swelling experiments. For each oocyte in the CO_2 and NH_3 assays (Figure 4 and Figure 7), we also determined P_f*. In Figure 8*A*, we summarize our AQP1-WT data, which confirm earlier work that shows that, in oocytes expressing AQP1-WT, mercurials reduce P_f* by about half (Macey, 1984; Preston *et al.*, 1993; Zeidel *et al.*, 1994; Musa-Aziz *et al.*, 2009*a*; Kabutomori *et al.*, 2018) but that DIDS is without effect (Macey, 1984; Endeward *et al.*, 2006). Figure 8*B* confirms that the AQP1-C189S mutation renders P_f* insensitive to pCMBS (Preston *et al.*, 1993; Cooper & Boron, 1998; Kabutomori *et al.*, 2018), and also shows that the mutation does not affect the lack of DIDS sensitivity.

Modification of AQP1 by DIDS

Via rapid and reversible electrostatic interactions, the two sulfonate groups of DIDS can reversibly interact with cationic sites on proteins. Via slower covalent reactions with the $–NH_2$ group of lysine or –OH/–SH groups of other amino acids, the two isothiocyanate groups of DIDS can act as a homobifunctional crosslinking reagent (Cabantchik & Rothstein, 1972; Lepke *et al.*, 1976).

pH_S experiments on oocytes. To assess whether the DIDS inhibition occurs via an electrostatic or covalent interaction, we followed a DIDS exposure with an albumin wash (see Methods) to scavenge non-covalently-bound DIDS. Figure 9*A* shows that the albumin wash does not significantly reduce the degree to which the DIDS pretreatment reduces decreases $(\Delta pH_S^*)_{CO_2}$. Because the inhibition is irreversible, the interaction of the DIDS with AQP1 is most likely covalent. To investigate this covalent modification, we performed the biochemistry experiments (presented in next section) in which we FLAG-tagged AQP1 at its N-terminus, overexpressed the construct in *Pichia pastoris,* and prepared spheroplasts. Here, in control oocyte experiments, we observe that the FLAG tag has no effect on the $(\Delta pH_S^*)_{CO_2}$, ±DIDS or ±albumin (Figure 9*B* vs. *A*). We also find that the FLAG tag is without effect in P_f assays, ±pCMBS or ±DIDS (Figure 9*D* vs. *C*).

Biochemistry experiments. In separate studies, as mentioned in the previous paragraph, we overexpressed FLAG-tagged AQP1 in *Pichia pastoris*, and prepared spheroplasts. We treated intact spheroplasts with DIDS (or, as shams, without DIDS), solubilized the membranes in

detergent, and purified AQP1 using an anti-FLAG resin. Further purification by size-exclusion chromatography (Figure 10*A*) shows that DIDS treatment promotes the formation of higher–molecular-weight AQP1 species, as indicated by the increased peak height of the void volume (V_0). We then pooled and concentrated fractions from each peak. Optical spectroscopy of this material (Figure 10*B*) reveals the expected increase in absorbance centered at ~340 nm (brown arrow; see Kodippili *et al.*, 2009), due to DIDS in the DIDS-treated vs. sham samples. We also separated the pooled/concentrated material by SDS-PAGE, and transferred to membranes for western blotting. In the anti-FLAG blot (Figure 10*C*), the dominant species are AQP1 monomers (≤50 kDa, arrows a–c) that, as we will see, represent mainly intracellular protein (i.e., not on plasma membrane). Presumed dimers (arrow d) and tetramers (arrow e) are visible only in DIDS-treated samples (lanes 2, 4, 6), and represent proteins accessible to DIDS at the outer cell surface. In the anti-DIDS blot (Figure 10*D*), the monomeric species (dominant in the anti-FLAG blot) are relatively poorly represented, whereas the presumed dimers and tetramers are clearly visible, though only for DIDS-treated samples (lanes 2, 4, 6). These data are consistent with the hypothesis that, once the divalent DIDS molecule reacts with one AQP1 monomer, the odds are high that the DIDS crosslinks to one more to yield dimers and tetramers. Although we attempted to use mass spectrometry to identify AQP1 residue(s) derivatized by DIDS, we were unable to achieve coverage of protein fragments containing predicted DIDS-reactive sites near hydrophobic transmembrane segments.

Discussion

Pathways for NH_3 vs. CO_2

NH_3 permeation through monomeric pores. Although previous work had shown that AQP1 can serve as a conduit for NH_3 (Nakhoul *et al.*, 2001), the present work is the first direct demonstration that the four monomeric pores of AQP1—which are responsible, of course, for all H_2O conductance (Preston *et al.*, 1993)—are, in fact, also responsible for all NH_3 conductance. This result is not unexpected, given the hydrophilicity of the monomeric pore (Walz *et al.*, 1997; Sui *et al.*, 2001; Tajkhorshid *et al.*, 2002), and the similarities of the electronic structures of the NH_3 molecule (i.e., 1 lone pair of electrons + 3 N–H bonds among 4 sp^3 hybrid orbitals) and the H_2O molecule (i.e., 2 lone pairs + 2 O–H bonds among 4 sp^3 hybrid orbitals). The primary evidence for our conclusion is that pCMBS reduces $(\Delta pH_S^*)_{NH_3}$ to zero (Figure 7*A*, bars 2 vs. 1), an effect abrogated by the C189S mutation (Figure 7*B*, bars 2 vs. 1). On the other hand, none of the NH_3 moves via the parallel DIDS-sensitive pathway, inasmuch as DIDS has no effect on $(\Delta pH_S^*)_{NH_3}$ (Figure 7*A* and *B*, bars 3 vs. 1). These results for NH_3 permeability parallel those for osmotic water permeability in Figure 8.

CO_2 permeation through monomeric pores. The present work confirms earlier observations (Cooper & Boron, 1998) that at least some CO_2 moves through AQP1 via the monomeric pore and, furthermore, shows that this pathway amounts to about half the total $(\Delta pH_S^*)_{CO_2}$ signal, or ~10% per monomeric pore. This result is not unexpected, given the amphiphilic nature of CO_2. Moreover, the molecular dynamics simulations of Wang et al (Wang *et al.*, 2007), suggest that 40% of the CO_2 permeability of AQP1 is due to the 4 monomeric pores (i.e., ~10% per monomeric pore). Evidence for this conclusion in the present study is that pCMBS reduces $(\Delta pH_S^*)_{CO_2}$ by somewhat more than half (Figure 4*A*, bars 2 vs. 1), an effect abrogated by the C189S mutation (Figure 4*B*, bars 2 vs. 1).

CO_2 permeation through a parallel pathway. The present work provides the first physiological evidence for a second pathway for CO_2 through the AQP1 tetramer—apparently parallel to the pathway through the four monomeric pores—that accounts for at least half of the total $(\Delta pH_S^*)_{CO_2}$ signal. The primary evidence is that (a) DIDS reduces $(\Delta pH_S^*)_{CO_2}$ by somewhat more than half in AQP1-WT (Figure 4*A*, bars 3 vs. 1), (b) the C189S mutation does not affect the DIDS blockade (Figure 4*B*, bars 3 vs. 1), and (c) the combination of pCMBS and DIDS reduces

$(\Delta pH_S^*)_{CO_2}$ to zero for oocytes expressing AQP1-WT (Figure 4*A*, bars 4 vs. 1), but still somewhat more than half for oocytes expressing AQP1-C189S (Figure 4*B*, bars 4 vs. 1).

Effect of Inhibitors

DIDS. Because the DIDS blockade is irreversible with both AQP1-WT (Figure 9*A*) and AQP1-FLAG (Figure 9*B*), DIDS probably interacts covalently with nearly all functional AQP1 tetramers on the oocyte surface. Indeed, with DIDS-treated cells, western blots probed with a DIDS antibody reveal presumed dimers and tetramers, but virtually no glycosylated monomers (Figure 10*C* and *D*). Thus, we conclude that one or more DIDS molecules, which are bivalent, most likely crosslink 2 or more monomers of virtually all AQP1 tetramers on the cell surface. If this crosslinking is essential for blockade, then the DIDS-sensitive component of CO_2 permeation would most likely reflect CO_2 movements between monomers, perhaps through the hydrophobic central pore. Indeed, the molecular dynamics simulations of Wang et al (Wang *et al.*, 2007) suggest that ~60% of the CO_2 permeability of AQP1 is due to the hydrophobic central pore—lined by residues (from extracellular to intracellular sides) Val-50, Leu-54, and Leu-58 from TM2, and Leu-174 and Leu-170 from TM5—that is largely devoid of H_2O. The mobility of a gas like CO_2 through such a near vacuum is ~10^4 higher than in liquid water (see Boron, 2010). Thus, even though central pores may comprise only a small fraction of total membrane surface area, it is possible that such pores—on the background of a membrane with a low intrinsic CO_2 permeability in the absence of AQP1 (Boron *et al.*, 2011)—could make a significant contribution to overall CO_2 permeability. We propose that the central pore is the anatomic substrate of the DIDS-sensitive component of CO_2 permeability of AQP1-WT.

Summing the effects of pCMBS and DIDS. The mathematical simulations of Somersalo *et al.* (2012) suggest that—in the region in which $(\Delta pH_S^*)_{CO_2}$ is most sensitive to the membrane permeability to CO_2 (P_{M,CO_2})—$(\Delta pH_S^*)_{CO_2}$ should rise linearly with the $\log(\Delta pH_S^*)_{CO_2}$ (see their figure A–B). Thus, if the pCMBS- or DIDS-induced decrease in $(\Delta pH_S^*)_{CO_2}$ were 50%, the fractional decrease in P_{M,CO_2} would be even greater. Thus, it is likely that blockade of the monomeric pore by pCMBS also reduces the CO_2 permeability of the parallel pathway (e.g., central pore), and that the blockade of this parallel pathway by DIDS also reduces the CO_2 permeability (but neither the H_2O or NH_3 permeability) of the monomeric pore. Such overlapping inhibition of CO_2 permeability would not be unreasonable inasmuch as the extracellular half of

TM2 not only lines the central pore, but also is in close proximity to selectivity filter and NPA motifs of the monomeric pore.

Molecular Basis of Gas Selectivity

NH_3. An important unresolved issue is the molecular basis for gas selectivity by AQPs (Musa-Aziz *et al.*, 2009*a*; Geyer *et al.*, 2013). Here we show that all NH_3 transits the 4 four hydrophilic monomeric pores of AQP1; that is, none moves via the parallel, hydrophobic pathway (e.g., central pore). Considering the broader family of AQPs, we predict that the hydrophobic parallel pathways (e.g., central pores) are never important routes of NH_3 conductance, but rather that the characteristics of the monomeric pores determine whether a particular AQP has a relatively high permeability to NH_3 (AQPs 3, 6, 7, 8, 9), or a relatively low NH_3 permeability (AQPs 2, 4, 5).

CO_2. The present study indicates that the amphiphilic CO_2 transits AQP1 via 2 pathways, the 4 hydrophilic monomeric pores and an alternate, more hydrophobic pathway (e.g., central pore). We suggest that, for the AQPs known to be permeable to CO_2 (AQPs 0, 4, 5, 6, 9), CO_2 transits a combination of monomeric pores and an alternate, more hydrophobic pathway. For the AQPs with limited CO_2 conductance (AQPs 2, 3, 7, 8), both monomeric pores and the parallel pathways presumably have less favorable physico-chemical characteristics. Because more-hydrophobic molecules like O_2 and N_2 are less likely to transit through the monomeric pores, their permeabilities likely depend exclusively on the physico-chemical characteristics of the alternate, hydrophobic pathway. Thus, the gas-selectivity profile of each AQP likely depends on the physico-chemical nature of each gas and the unique set of physico-chemical properties of the (at least 2) potential pathways through the tetramer.

Concluding Remarks

Our work establishes the proof of principle for blocking the parallel pathways, at least somewhat independently. Elimination of the monomeric pathway, combined with judicious mutations to the hydrophobic alternate pathway, could enable the design of channels with exquisite selectivity among gases. Such designer channels could revolutionize certain industrial processes, provide a simple approach for venting metabolically produced CO_2 in diving or space flight, and optimize CO_2 and N_2 conduction in agriculture.

Additional information

Competing interests

All authors declare no conflict of interests.

Authors' contributions

R.M-A contributed to the conception and design of the research; performed all the oocyte experiments; analyzed and interpreted all the results collected with oocytes; prepared the figures; wrote and edited the manuscript. R.R.G contributed to the conception and design of the research related to *Pichia pastoris*; performed all the *Pichia pastoris* experiments; analyzed and interpreted all the results collected with *Pichia pastoris*; prepared the figures; wrote the manuscript. F.J.M performed statistical analyses and edited the manuscript. W.F.B contributed to the conception and design of the research; wrote and edited the manuscript.

All authors approved the final version of the manuscript and all qualify for authorship, and all those who qualify for authorship are listed.

Funding

R Musa-Aziz was supported for parts of this project by Fundação de Amparo a Pesquisa do Estado de São Paulo (FAPESP # 13/11364-3 and 18/22855-1). RR Geyer was supported by postdoctoral fellowship N00014-09-1-0246 from the Office of Naval Research. This work was supported by National Institutes of Health Grants NS-18400, DK-8156, HL-160857 and U54-GM087519, as well as Office of Naval Research Grants N00014-05-1-0345, N00014-08-1-0532, and N00014-11-1-0889.

Acknowledgements

We thank Duncan Wong for helpful discussions and computer support; Dale Huffman for engineering assistance and helpful discussions; We thank Steven Torontali for designing and fabricating the oocyte chamber; Gerald Babcock for technical assistance and laboratory management; Morley Schwebel for administrative support; Rosalyn Forster and Lesa Goodman for administrative support. W. F. Boron gratefully acknowledges the support of the Myers/Scarpa endowed chair. R. Musa-Aziz gratefully thanks Dr. Mark D. Parker (University at Buffalo: State

University of New York), Dr. Seong-Ki Lee (Case Western Reserve University, Cleveland, OH) for helpful discussions, and gives special thanks in memory of Dr. Gerhard Malnic (University of São Paulo, SP, BR), for his unwavering support and advice.

Supporting information

N/A

Data Availability Statement

The data that support the findings of this study are available from the corresponding author upon reasonable request.

Figure legends

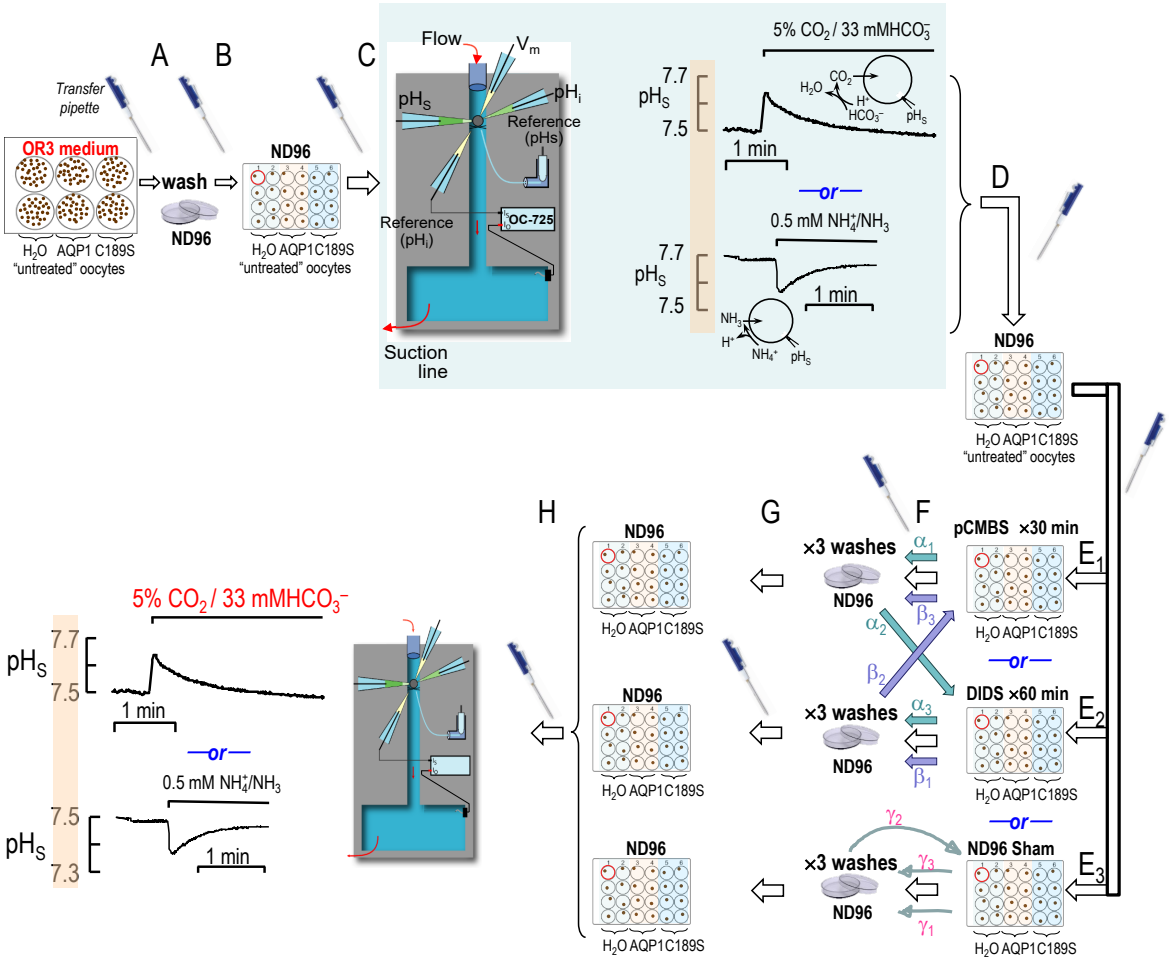

Figure 1: Flow chart showing experimental protocols. The letters "A", "B", "C" and so on are above broad arrows and near icons of a pipetter that identify the transfer of an oocyte (using a transfer pipette) from one step in our protocol to another. The oocytes may be controls (injected with H_2O) or those expressing either AQP1-WT (AQP1) or AQP1-C189S (C189S). In transfer "E", we move the oocyte to a solution containing pCMBS (E_1), DIDS pCMBS (E_2), or no drug (E_3). As indicated by the white arrows, we can execute the direct transfers E_{123}→F→G. Alternatively, at transfer "F", we can execute subsidiary protocols (α/teal, β/lavender, γ/gray arrows) in which we return oocytes from washes in ND96 back to a solution containing an inhibitor (i.e., pCMBS or DIDS) or ND96 (i.e., sham drug exposure). Thus, an oocyte might undergo the teal-colored pCMBS/DIDS

sequence ($\alpha_1 \rightarrow \alpha_2 \rightarrow \alpha_3$), the lavender-colored DIDS/pCMBS sequence ($\beta_1 \rightarrow \beta_2 \rightarrow \beta_3$), or the gray-colored Sham/Sham sequence ($\gamma_1 \rightarrow \gamma_2 \rightarrow \gamma_3$).

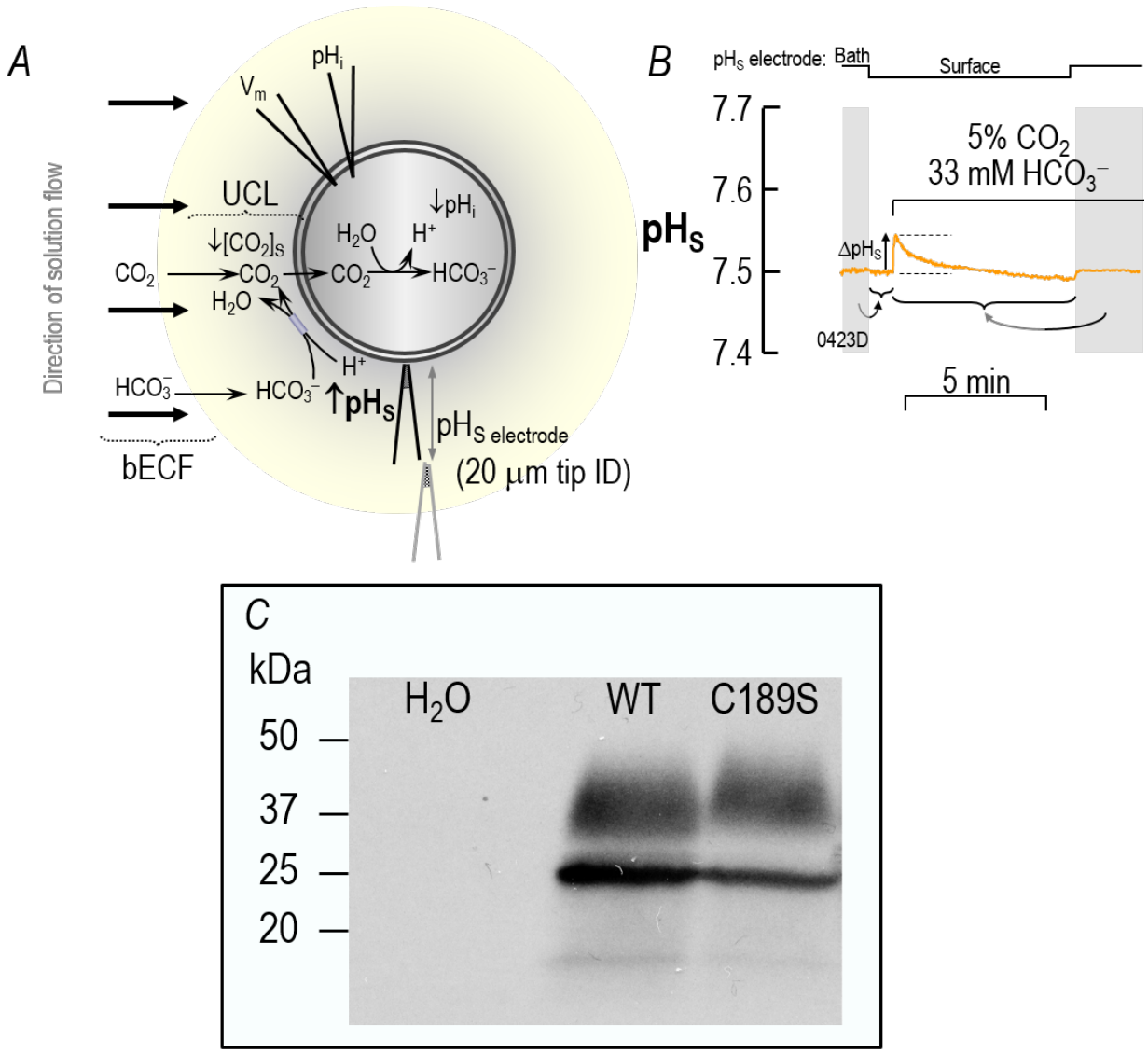

Figure 2: CO_2 influx into an oocyte. *A,* schematic illustration of a CO_2-influx experiment. Thick black arrow indicates direction of convective flow within the bulk extracellular fluid (bECF). Thinner arrows indicate diffusion of solutes or reactions. The maize-colored halo indicates the layer of extracellular unconvected fluid (EUF). At the outer surface of the membrane, CO_2 influx creates a CO_2 deficit, in part replenished by the reaction $HCO_3^- + H^+ \rightarrow CO_2 + H_2O$ (which raises pH_S) and in part replenished by diffusion from the bECF

(which is isohydric). The double-headed arrow indicates movement of the pH_S electrode from the bECF to the cell surface. *B,* sample surface-pH (pH_S record). The upward arrow indicates the maximal change in pH_S (ΔpH_S) during the application of CO_2/HCO_3^-. During the two periods indicated by the vertical gray bands, the tip of the pH_S electrode was about 300 μm away from the cell surface, for calibration in the bulk extracellular fluid (i.e., pH = 7.50). The curved gray arrows points to horizontal braces that indicate the portions of the experiment to which each calibration pertains. *C,* western blot, probed with an anti-AQP1 antibody, showing relative expression of AQP1-WT vs. AQP1-C189S in one of 3 membrane preparation of oocytes.; ID, inner diameter.

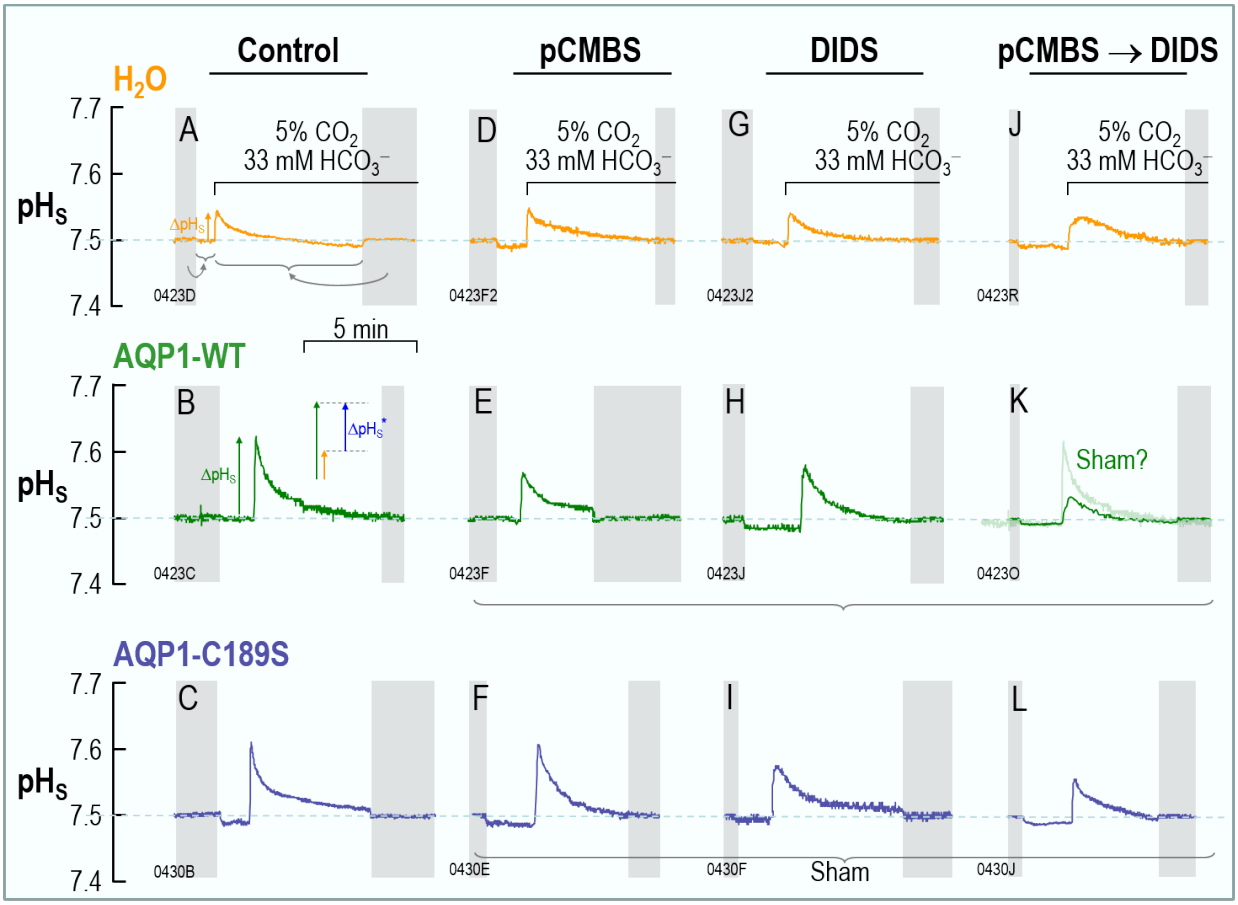

Figure 3: Surface-pH transients triggered by a CO_2/HCO_3^- exposure and subsequent CO_2 influx

The figure shows representative pH_S records from oocytes injected with H_2O (top row) or cRNA encoding AQP1 (middle row) or its C189S mutant (bottom row), and later exposed first to the ND96 solution and then, at the indicated times, to a solution containing CO_2/HCO_3^-. All oocytes underwent the "Control" protocol, followed by one or two of the three indicated drug protocols (see Methods and Figure 1), although some did not survive beyond the control protocol. As necessary, we pre-incubated oocytes in 1 mM pCMBS for 30 minutes, or in 100 μM DIDS for 1 hour. Neither drug was present in the bulk solution at the time of the assays. The two gray bars in each panel indicate when we withdrew the pH-electrode tip from the oocyte surface to the bulk extracellular fluid (pH 7.50) for recalibration. In panel *A*, the curved gray arrows points and horizontal braces have the

same meanings as in Figure 2*B*, and the upward gold arrow indicates the control ΔpH_S. In panel *B*, the upward green arrow indicates the ΔpH_S in an oocyte expressing AQP1. The inset shows that the difference in heights of the green arrow and the gold arrow (its day-matched control) is the channel-dependent ΔpH_S (ΔpH_S*).

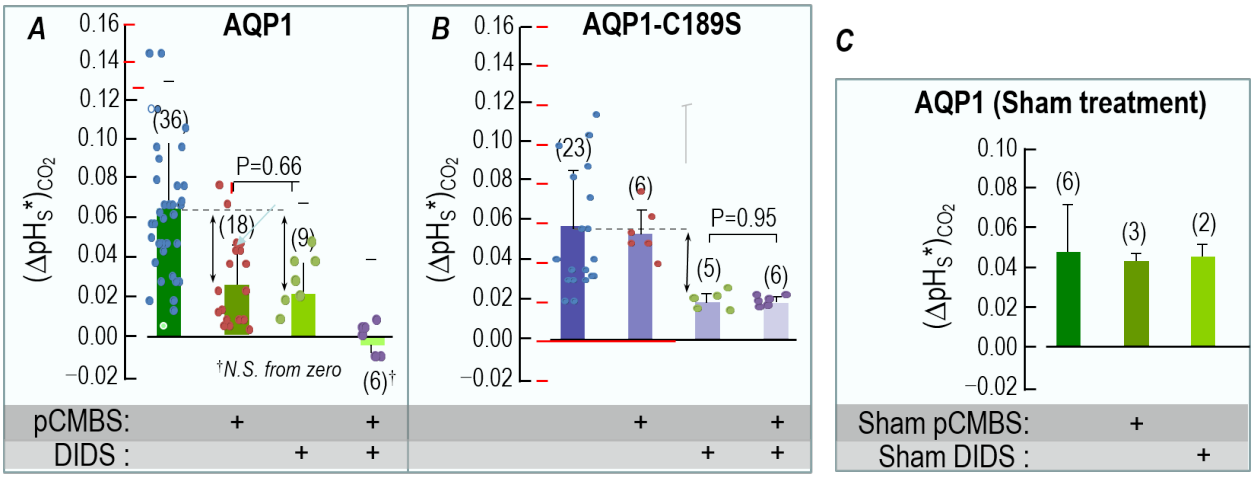

Figure 4: Summary of channel-specific data in assays for CO_2 influx

A, oocytes expressing AQP1. *B,* oocytes expressing the C189S mutant of AQP1. *C,* oocytes expressing AQP1 but undergoing sham drug exposures. The data come from experiments like those in Figure 3, in which we exposed oocytes to 5% CO_2/33 mM HCO_3^- (for protocol, see Methods and Figure 1). For each ΔpH_S from a channel-expressing oocyte (e.g., Figure 3*B*, *E*, *H*, *K* or *C*, *F*, *I*, *L*), we subtracted the mean, day-matched ΔpH_S for the corresponding H_2O-injected oocytes (e.g., Figure 3*A*, *D*, *G*, and *J*). Green- and purple-shaded vertical bars represent mean subtracted values: the channel-dependent ΔpH_S for CO_2, that is, $(\Delta pH_S^*)_{CO_2}$. In the horizontal gray bands at the bottom of each panel, "+" indicates an exposure to pCMBS or DIDS, or a sham exposure. These results show that in AQP1-WT oocytes (panel *A*), pCMBS and DIDS each reduces $(\Delta pH_S^*)_{CO_2}$ by somewhat more than half, and the two drugs together reduce it to virtually zero. In AQP1-C189S oocytes (panel *B*), DIDS still reduces $(\Delta pH_S^*)_{CO_2}$ by about half, but pCMBS is without effect, ±DIDS. The sham experiments (panel *C*) show that the long protocols did not have a substantial effect on $(\Delta pH_S^*)_{CO_2}$. In panel *B*, the +pCMBS experiments are effectively shams because AQP1-C189S is insensitive to pCMBS. In parentheses are the numbers of oocytes, which come from a minimum of 5 batches of oocytes (i.e., different frogs). Error bars represent SD. For the rightmost bar in panel *A*, we treated oocytes in the order pCMBS→DIDS (see Figure 1, step G, α pathway), and in the opposite order (β pathway). In panel *B*, oocytes followed the α pathway, and the β pathway. P values are

results of one-way ANOVAs among all groups, followed by Student-Newman-Keuls analyses.

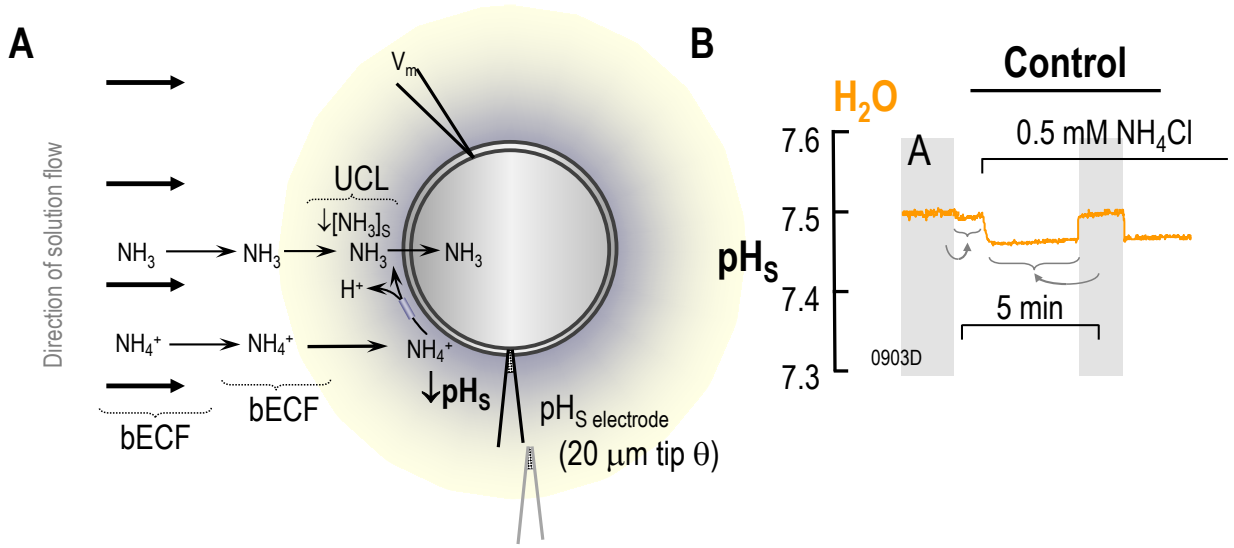

Figure 5: Panel A shows the NH_3 influx into an oocyte. Exposing an oocyte to a solution containing NH_3/NH_4^+ generates a transient fall in pH_S as the weak base NH_3 enters the cell. **Panel B shows a representative experiment with H_2O-injected control 1.oocyte**. At the indicated times, we switched the extracellular solution from ND96 to 0.5 mM NH_3/NH_4^+. The vertical gray bands represent periods during which the pH_S electrode was moved to the bulk ECF for calibration (fixed pH of 7.50).

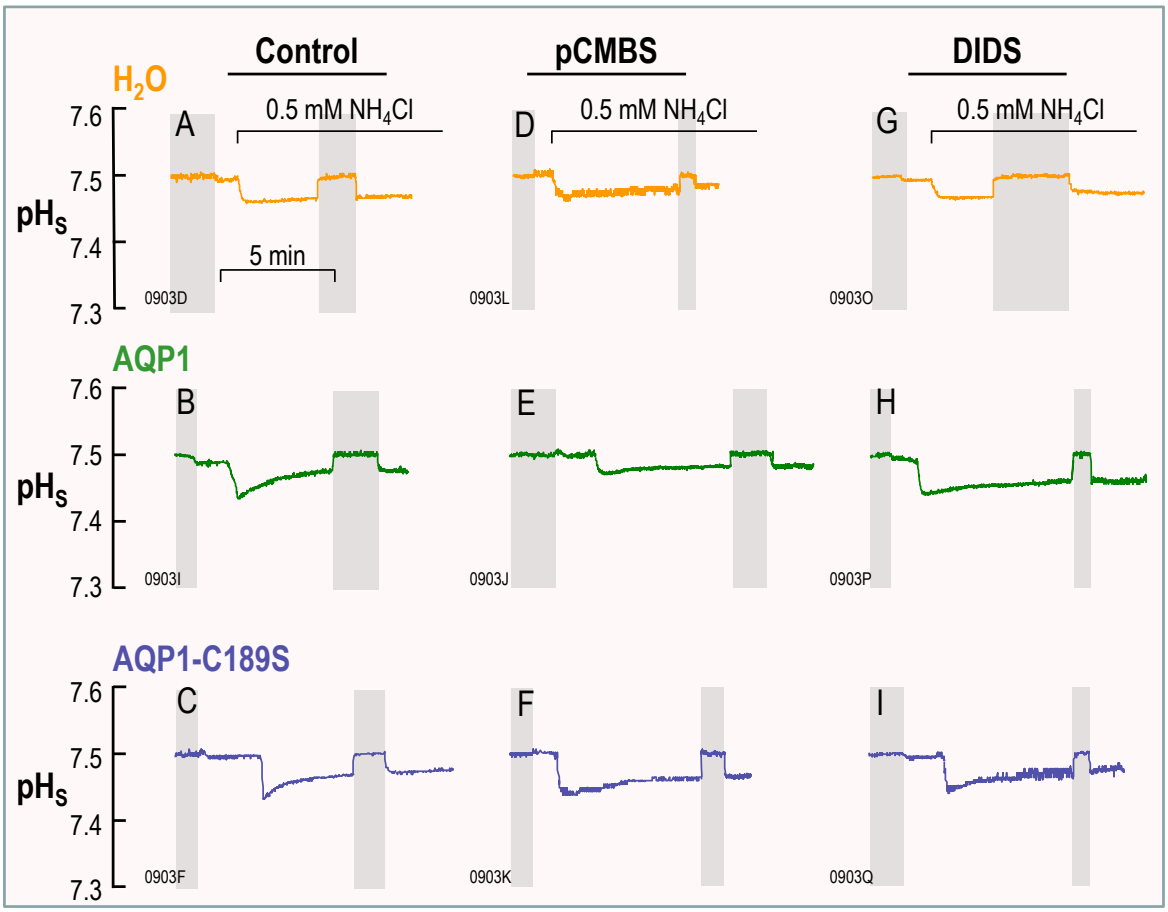

Figure 6: Surface-pH transients triggered by NH_3/NH_4^+ exposure and the subsequent NH_3 influx

At the outer surface of the membrane, the NH_3 influx creates an NH_3 deficit, in part replenished by the reaction $NH_4^+ \rightarrow NH_3 + H^+$, which lowers pH_S. The figure shows representative pH_S records from oocytes injected with H_2O (top row) or cRNA encoding AQP1 (middle row) or its C189S mutant (bottom row), and later exposed first to the ND96 solution and then, at the indicated times, to a solution containing NH_3/NH_4^+. All oocytes underwent the "Control" protocol, followed by one of the two indicated drug protocols, although some did not survive beyond the control protocol (see Methods). As necessary, we pre-incubated oocytes in 1 mM pCMBS for 30 minutes, or in 100 μM DIDS for 1 hour. Neither drug was present in the bulk solution at the time of the assays. The gray bars indicate when we withdrew the pH-electrode tip from the oocyte surface to the bulk extracellular solution (pH 7.50) for recalibration.

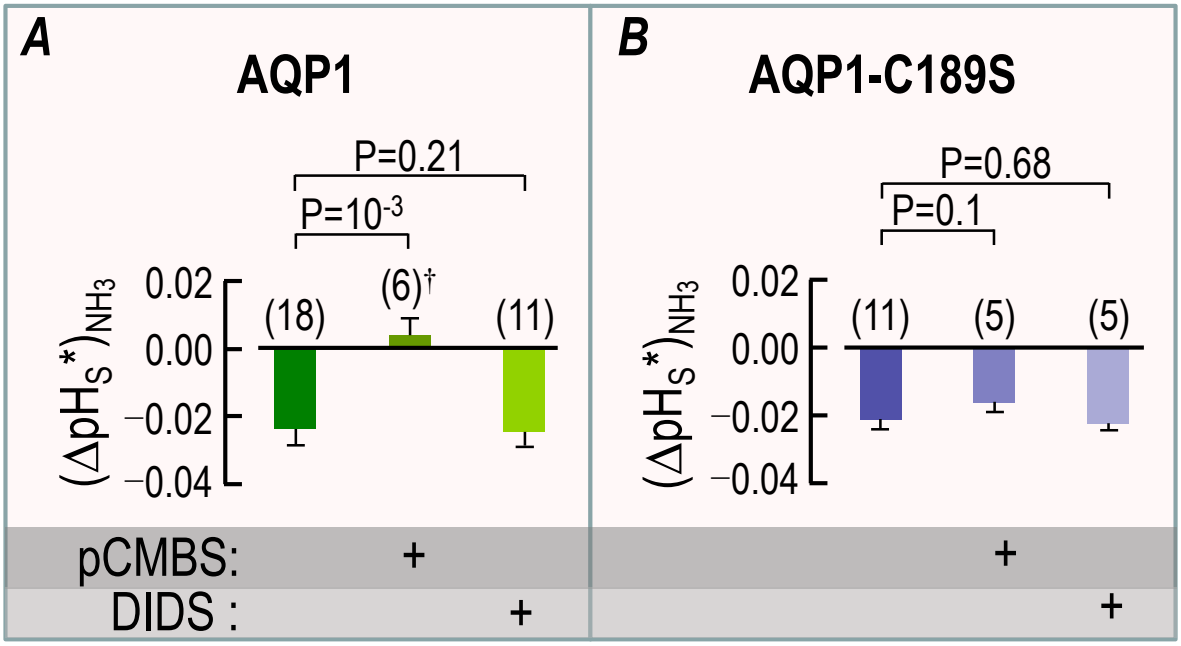

Figure 7: Summary of channel-specific data in assays for NH_3 influx

The data come from experiments like those in Figure 6, in which we exposed oocytes to 0.5 mM NH_4Cl. For each ΔpH_S from a channel-expressing oocyte (Figure 6*B*, *E*, *H* or *C, F, I*), we subtracted the corresponding mean, day-matched ΔpH_S for H_2O-injected oocytes (Figure 6*A, D, G*). Bars represent mean subtracted values: the channel-dependent ΔpH_S for NH_3, that is, $(\Delta pH_S^*)_{NH_3}$. These results show that in AQP1-WT, pCMBS but not DIDS reduces P_f to nearly zero, whereas in AQP1-C189S, neither drug affects P_f. Presence of pCMBS or DIDS is indicated by "+" in the bands beneath the bars. In parentheses is the number of oocytes, which come from a minimum of 5 batches of oocytes (i.e., different frogs). Error bars represent SEM. P values are results of one-way ANOVAs among all groups, followed by Student-Newman-Keuls analyses.

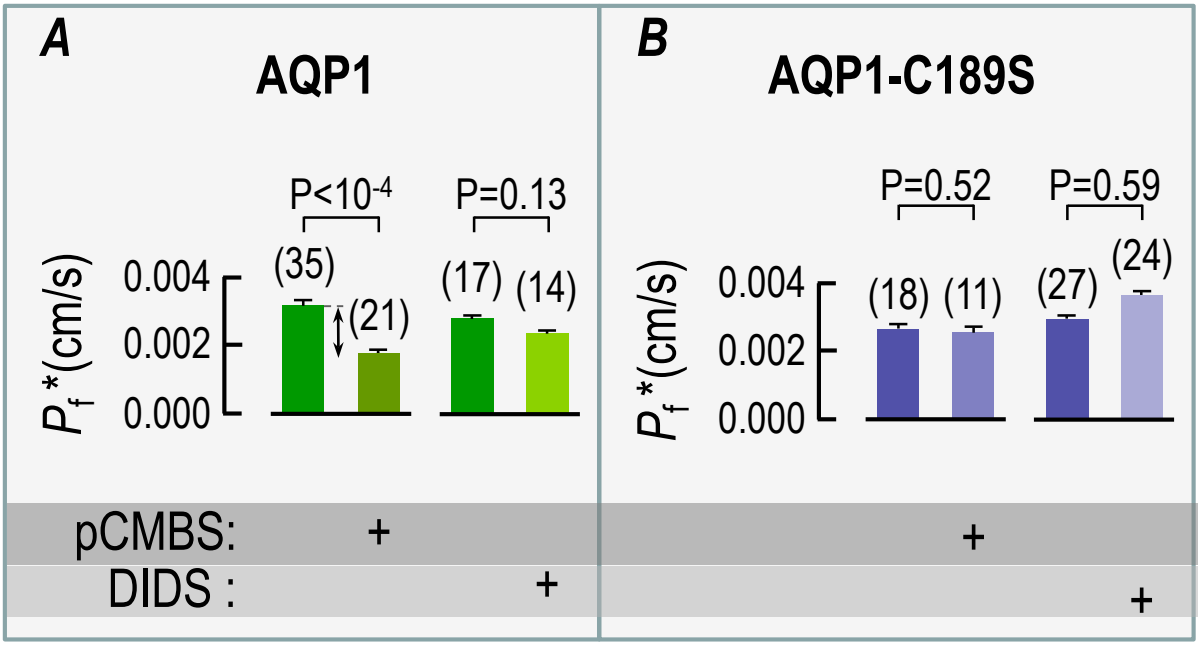

Figure 8: Summary of channel-specific data in assays for osmotic water permeability

For each P_f from a channel-expressing oocyte, we subtracted the mean, day-matched or P_f for H_2O-injected oocytes. Colored bars represent mean subtracted values: the channel-dependent P_f, that is, P_f*. These results show that pCMBS but not DIDS reduces P_f. Presence of pCMBS or DIDS is indicated by "+" in the bands beneath the bars. In parentheses is the number of oocytes, which come from a minimum of 5 batches of oocytes (i.e., different frogs). Error bars represent SEM. P values are results of one-way ANOVAs among all groups, followed by Student-Newman-Keuls analyses.

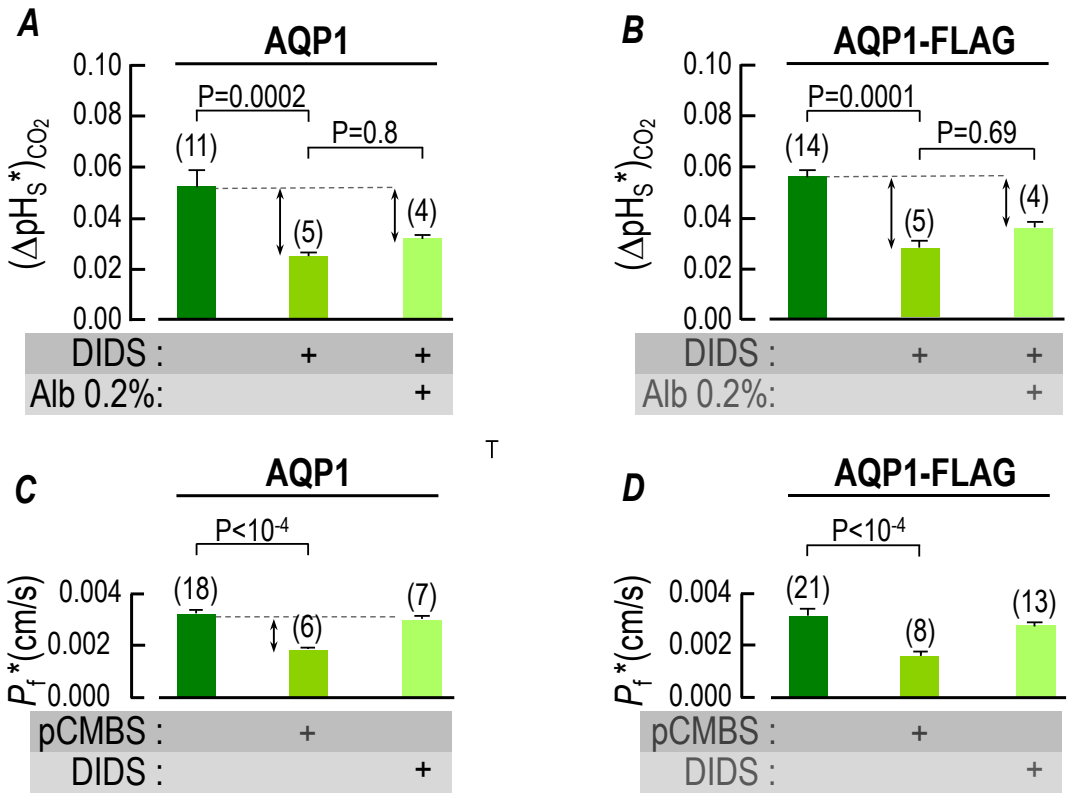

Figure 9: Summary of channel-specific data for CO_2 and H_2O influx for WT vs. FLAG-tagged AQP1

For panels *A* and *B* , the control pH_S data (leftmost bars) come from experiments like those in Figure 3, whereas for panels *C* and *D* , the control P_f data come from experiments like those in in 8.

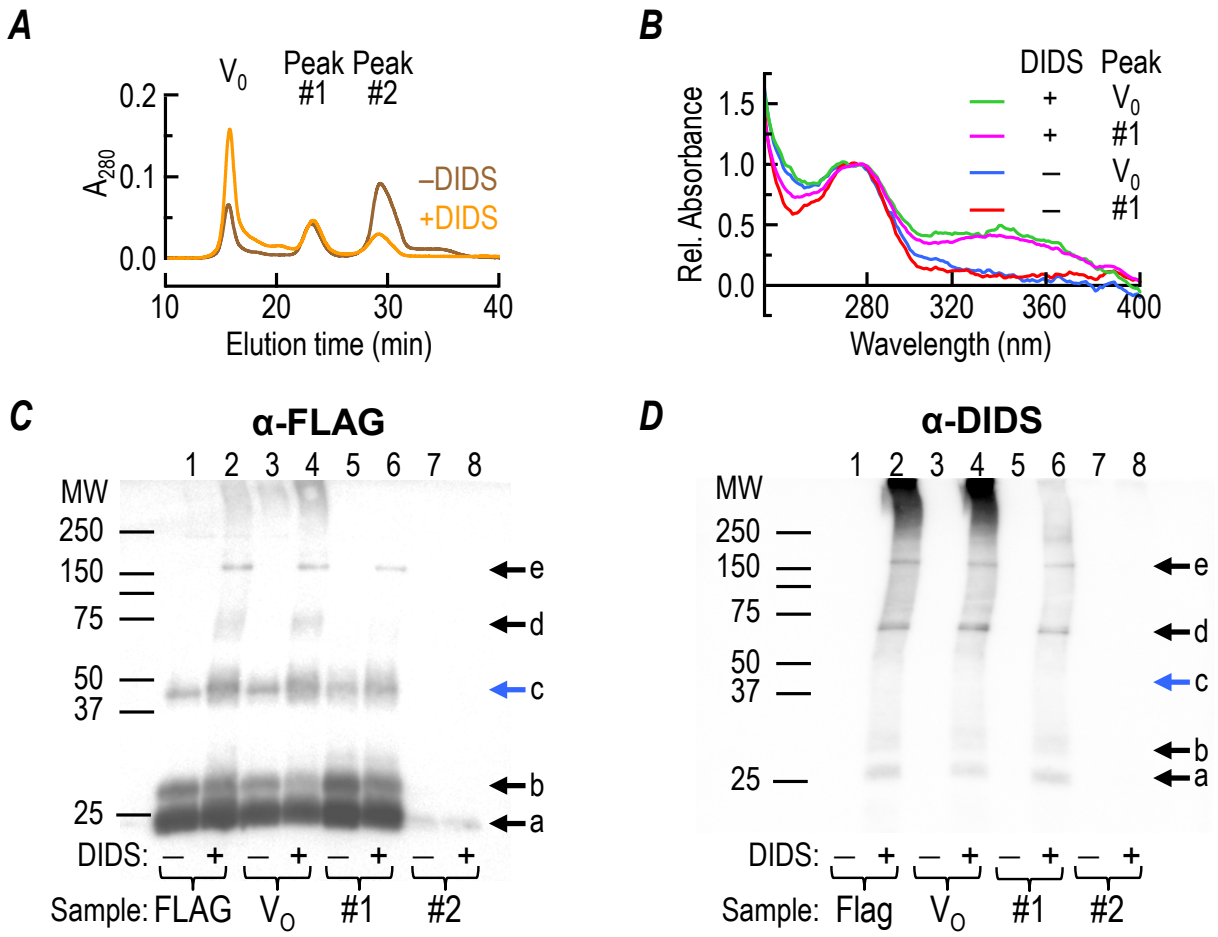

Figure 10: Reaction of DIDS with hAQP1 overexpressed in *Pichia pastoris*.

A, Size-exclusion chromatography of solubilized proteins. We treated spheroplasts with DIDS (or no DIDS in parallel, sham experiments), solubilized with DMM, purified AQP1 using an anti-FLAG column, and then separated by FPLC on a Superdex-200 column, recording A_{280} vs. time. The green record represents a DIDS-treated sample and the red record, a control sample from the same preparation. The first peaks are the void volume (V_0), which consists of high molecular-weight (MW) proteins. Peak #1 consists of lower-MW proteins, and Peak #2, even smaller ones. We translated both records to so that A_{280} averaged zero between 10 and 13 min, and then we scaled the +DIDS record to that it has the same area under the curve as the –DIDS record. *B,* Absorbance spectra of material (±DIDS) from peaks V_0 and #1, from a preparation similar to that shown in panel *A*. We normalized all spectra to unity at 280 nm. The increased absorbance from ~320 to ~370 nm in the DIDS-treated samples presumably represents DIDS, which has an

absorbance peak at ~340 nm (Kodippili *et al.*, 2009). *C,* Western blot of material from the same experiment as in panel *B*, probed with anti-FLAG: Lane 1. Material obtained from spheroplasts not treated with DIDS, and purified on anti-FLAG column, as described for panel *A*, but not subjected to size-exclusion chromatography. ||| Lane 2. Same as Lane 1, but from DIDS-treated spheroplasts ||| Lane 3. Peak V_0 from spheroplasts –DIDS ||| Lane 4. Same as Lane 3, but from spheroplasts +DIDS ||| Lane 5. Peak #1 from spheroplasts –DIDS ||| Lane 6. Same as Lane 5, but from spheroplasts +DIDS ||| Lane 7. Peak #2 from spheroplasts –DIDS ||| Lane 8. Same as Lane 7, but from spheroplasts +DIDS. The presumed assignments are: "a" band < 25 kDa, unglycosylated AQP1 monomer cleaved at the C terminus; band "b", 28 kDa, full-length unglycosylated monomer; band "c", glycosylated monomer; band "d", glycosylated dimer; band "e", glycosylated tetramer. *D,* Western blot of material from the same experiment as in panels *B* and *C*, probed with anti-DIDS. The lane assignments are the same as in panel *C*. The results in panels *A* through *D* are representative of two independent experiments.

References

Ammann D, Lanter F, Steiner RA, Schulthess P, Shijo Y & Simon W (1981). Neutral carrier based hydrogen ion selective microelectrode for extra- and intracellular studies. *Anal Chem* **53,** 2267–2269.

Assentoft M, Kaptan S, Schneider H-P, Deitmer JW, de Groot BL & MacAulay N (2016). Aquaporin 4 as a NH_3 channel. *J Biol Chem* **291,** 19184–19195.

Becker HM & Deitmer JW (2007). Carbonic anhydrase II increases the activity of the human electrogenic Na^+/HCO_3^- cotransporter. *J Biol Chem* **282,** 13508–13521.

Boron WF (2010). Sharpey-Schafer lecture: gas channels. *Exp Physiol* **95,** 1107–1130.

Boron WF, Endeward V, Gros G, Musa-Aziz R & Pohl P (2011). Intrinsic CO_2 permeability of cell membranes and potential biological relevance of CO_2 channels. *Chemphyschem Eur J Chem Phys Phys Chem* **12,** 1017–1019.

Cabantchik ZI & Rothstein A (1972). The nature of the membrane sites controlling anion permeability of human red blood cells as determined by studies with disulfonic stilbene derivatives. *J Membr Biol* **10,** 311–330.

Calvetti D, Prezioso J, Occhipinti R, Boron WF & Somersalo E (2020). Computational model of electrode-induced microenvironmental effects on pH measurements near a cell membrane. *SIAM Multiscale Model Simul* **18,** 1053–1075.

Cooper GJ & Boron WF (1998). Effect of pCMBS on CO_2 permeability of *Xenopus* oocytes expressing aquaporin 1 or its C189S mutant. *Am J Physiol* **275,** C1481-1486.

Endeward V, Cartron J-P, Ripoche P & Gros G (2008). RhAG protein of the Rhesus complex is a CO_2 channel in the human red cell membrane. *FASEB J* **22,** 64–73.

Endeward V, Musa-Aziz R, Cooper GJ, Chen L-M, Pelletier MF, Virkki LV, Supuran CT, King LS, Boron WF & Gros G (2006). Evidence that aquaporin 1 is a major pathway for CO_2 transport across the human erythrocyte membrane. *FASEB J* **20,** 1974–1981.

Forster RE, Gros G, Lin L, Ono Y & Wunder M (1998). The effect of 4,4'-diisothiocyanato-stilbene-2,2'-disulfonate on CO_2 permeability of the red blood cell membrane. *Proc Natl Acad Sci U S A* **95,** 15815–15820.

Garcia AM & Lodish HF (1989). Lysine 539 of human band 3 is not essential for ion transport or inhibition by stilbene disulfonates. *J Biol Chem* **264,** 19607–19613.

Geyer RR, Musa-Aziz R, Qin X & Boron WF (2013). Relative CO_2/NH_3 selectivities of mammalian aquaporins 0-9. *Am J Physiol Cell Physiol* **304,** C985-994.

Gomes D, Agasse A, Thiébaud P, Delrot S, Gerós H & Chaumont F (2009). Aquaporins are multifunctional water and solute transporters highly divergent in living organisms. *Biochim Biophys Acta* **1788,** 1213–1228.

Herrera M, Hong NJ & Garvin JL (2006). Aquaporin-1 transports NO across cell membranes. *Hypertension* **48,** 157–164.

Kabutomori J, Beloto-Silva O, Geyer RR & Musa-Aziz R (2018). Lithobates catesbeianus (American Bullfrog) oocytes: a novel heterologous expression system for aquaporins. *Biol Open*; DOI: 10.1242/bio.031880.

Kodippili GC, Spector J, Sullivan C, Kuypers FA, Labotka R, Gallagher PG, Ritchie K & Low PS (2009). Imaging of the diffusion of single band 3 molecules on normal and mutant erythrocytes. *Blood* **113,** 6237–6245.

Leduc-Nadeau A, Lahjouji K, Bissonnette P, Lapointe J-Y & Bichet DG (2007). Elaboration of a novel technique for purification of plasma membranes from Xenopus laevis oocytes. *Am J Physiol Cell Physiol* **292,** C1132-1136.

Lepke S, Fasold H, Pring M & Passow H (1976). A study of the relationship between inhibition of anion exchange and binding to the red blood cell membrane of 4,4'-diisothiocyano stilbene-2,2'-disulfonic acid (DIDS) and its dihydro derivative (H_2DIDS). *J Membr Biol* **29,** 147–177.

Lu J, Daly CM, Parker MD, Gill HS, Piermarini PM, Pelletier MF & Boron WF (2006). Effect of human carbonic anhydrase II on the activity of the human electrogenic Na/HCO_3^- cotransporter NBCe1-A in *Xenopus* oocytes. *J Biol Chem* **281,** 19241–19250.

Macey RI (1984). Transport of water and urea in red blood cells. *Am J Physiol* **246,** C195-203.

Michenkova M, Taki S, Blosser MC, Hwang HJ, Kowatz T, Moss FJ, Occhipinti R, Qin X, Sen S, Shinn E, Wang D-K, Zeise B, Zhao P, Malmstadt N, Vahedi-Faridi A, Tajkhorshid E & Boron WF (2021). Carbon dioxide transport across membranes. *Interface Focus* **11,** 2.

Musa-Aziz R, Boron WF & Parker MD (2010). Using fluorometry and ion-sensitive microelectrodes to study the functional expression of heterologously-expressed ion channels and transporters in *Xenopus* oocytes. *Methods San Diego Calif* **51,** 134–145.

Musa-Aziz R, Chen L-M, Pelletier MF & Boron WF (2009*a*). Relative CO_2/NH_3 selectivities of AQP1, AQP4, AQP5, AmtB, and RhAG. *Proc Natl Acad Sci U S A* **106,** 5406–5411.

Musa-Aziz R, Jiang L, Chen L-M, Behar KL & Boron WF (2009*b*). Concentration-dependent effects on intracellular and surface pH of exposing *Xenopus* oocytes to solutions containing NH_3/NH_4^+. *J Membr Biol* **228,** 15–31.

Musa-Aziz R, Occhipinti R & Boron WF (2014*a*). Evidence from simultaneous intracellular- and surface-pH transients that carbonic anhydrase II enhances CO_2 fluxes across *Xenopus* oocytes plasma membranes. *Am J Physiol Cell Physiol* **307,** C791-813.

Musa-Aziz R, Occhipinti R & Boron WF (2014*b*). Evidence from simultaneous intracellular- and surface-pH transients that carbonic anhydrase IV enhances CO_2 fluxes across *Xenopus* oocyte plasma membranes. *Am J Physiol Cell Physiol* **307,** C814-840.

Nakhoul NL, Davis BA, Romero MF & Boron WF (1998). Effect of expressing the water channel aquaporin-1 on the CO_2 permeability of *Xenopus* oocytes. *Am J Physiol* **274,** C543-548.

Nakhoul NL, Hering-Smith KS, Abdulnour-Nakhoul SM & Hamm LL (2001). Transport of NH_3/NH_4^+ in oocytes expressing aquaporin-1. *Am J Physiol Renal Physiol* **281,** F255-263.

Occhipinti R, Musa-Aziz R & Boron WF (2014). Evidence from mathematical modeling that carbonic anhydrase II and IV enhance CO_2 fluxes across *Xenopus* oocytes plasma membranes. *Am J Physiol Cell Physiol* **307,** C841-858.

Prasad GV, Coury LA, Finn F & Zeidel ML (1998). Reconstituted aquaporin 1 water channels transport CO_2 across membranes. *J Biol Chem* **273,** 33123–33126.

Preston GM & Agre P (1991). Isolation of the cDNA for erythrocyte integral membrane protein of 28 kilodaltons: member of an ancient channel family. *Proc Natl Acad Sci U S A* **88,** 11110–11114.

Preston GM, Carroll TP, Guggino WB & Agre P (1992). Appearance of water channels in *Xenopus* oocytes expressing red cell CHIP28 protein. *Science* **256,** 385–387.

Preston GM, Jung JS, Guggino WB & Agre P (1993). The mercury-sensitive residue at cysteine 189 in the CHIP28 water channel. *J Biol Chem* **268,** 17–20.

Roos A & Boron WF (1981). Intracellular pH. *Physiol Rev* **61,** 296–434.

Somersalo E, Occhipinti R, Boron WF & Calvetti D (2012). A reaction-diffusion model of CO_2 influx into an oocyte. *J Theor Biol* **309,** 185–203.

Sui H, Han BG, Lee JK, Walian P & Jap BK (2001). Structural basis of water-specific transport through the AQP1 water channel. *Nature* **414,** 872–878.

Tajkhorshid E, Nollert P, Jensen MØ, Miercke LJW, O'Connell J, Stroud RM & Schulten K (2002). Control of the selectivity of the aquaporin water channel family by global orientational tuning. *Science* **296,** 525–530.

Trudeau MC, Warmke JW, Ganetzky B & Robertson GA (1995). HERG, a human inward rectifier on the voltage-gated potassium channel family. *Science* **269,** 92–95.

Uehlein N, Lovisolo C, Siefritz F & Kaldenhoff R (2003). The tobacco aquaporin NtAQP1 is a membrane CO_2 pore with physiological functions. *Nature* **425,** 734–737.

Verkman AS (2008). Mammalian aquaporins: diverse physiological roles and potential clinical significance. *Expert Rev Mol Med* **10,** e13.

Verkman AS, Ruiz-Ederra J & Levin MH (2008). Functions of aquaporins in the eye. *Prog Retin Eye Res* **27,** 420–433.

Virkki LV, Cooper GJ & Boron WF (2001). Cloning and functional expression of an MIP (AQP0) homolog from killifish (Fundulus heteroclitus) lens. *Am J Physiol Regul Integr Comp Physiol* **281,** R1994-2003.

Waisbren SJ, Geibel JP, Modlin IM & Boron WF (1994). Unusual permeability properties of gastric gland cells. *Nature* **368,** 332–335.

Walz T, Hirai T, Murata K, Heymann JB, Mitsuoka K, Fujiyoshi Y, Smith BL, Agre P & Engel A (1997). The three-dimensional structure of aquaporin-1. *Nature* **387,** 624–627.

Wang C, Hu H, Qin X, Zeise B, Xu D, Rappel W-J, Boron WF & Schroeder JI (2016). Reconstitution of CO_2 regulation of SLAC1 anion channel and function of CO_2-permeable PIP2;1 aquaporin as carbonic anhydrase 4 interactor. *Plant Cell* **28,** 568–582.

Wang Y, Cohen J, Boron WF, Schulten K & Tajkhorshid E (2007). Exploring gas permeability of cellular membranes and membrane channels with molecular dynamics. *J Struct Biol* **157,** 534–544.

Zeidel ML, Nielsen S, Smith BL, Ambudkar SV, Maunsbach AB & Agre P (1994). Ultrastructure, pharmacologic inhibition, and transport selectivity of aquaporin channel-forming integral protein in proteoliposomes. *Biochemistry* **33,** 1606–1615.

Zhang RB, Logee KA & Verkman AS (1990). Expression of mRNA coding for kidney and red cell water channels in *Xenopus* oocytes. *J Biol Chem* **265,** 15375–15378.